PCCP

PAPER

Cite this: *Phys. Chem. Chem. Phys.*, 2017, **19**, 15780

A vacuum ultraviolet photoionization study on high-temperature decomposition of JP-10 (*exo*-tetrahydrodicyclopentadiene)†

Long Zhao,[a] Tao Yang,[a] Ralf I. Kaiser, *[a] Tyler P. Troy,[b] Bo Xu,[b] Musahid Ahmed, *[b] Juan Alarcon,[c] Daniel Belisario-Lara,[c] Alexander M. Mebel, *[c] Yan Zhang,[d] Chuangchuang Cao[d] and Jiabiao Zou[e]

Received 11th March 2017,
Accepted 4th May 2017

DOI: 10.1039/c7cp01571b

rsc.li/pccp

Two sets of experiments were performed to unravel the high-temperature pyrolysis of tricyclo[5.2.1.$0^{2,6}$] decane (JP-10) exploiting high-temperature reactors over a temperature range of 1100 K to 1600 K, Advanced Light Source (ALS), and 927 K to 1083 K, National Synchrotron Radiation Laboratory (NSRL), with residence times of a few tens of microseconds (ALS) to typically 144 ms (NSRL). The products were identified *in situ* in supersonic molecular beams *via* single photon vacuum ultraviolet (VUV) photoionization coupled with mass spectroscopic detection in a reflectron time-of-flight mass spectrometer (ReTOF). These studies were designed to probe the initial (ALS) and also higher order reaction products (NSRL) formed in the decomposition of JP-10 – including radicals and thermally labile closed-shell species. Altogether 43 products were detected and quantified including C1–C4 alkenes, dienes, C3–C4 cumulenes, alkynes, eneynes, diynes, cycloalkenes, cyclo-dienes, aromatic molecules, and most importantly, radicals such as ethyl, allyl, and methyl produced at shorter residence times. At longer residence times, the predominant fragments were molecular hydrogen (H_2), ethylene (C_2H_4), propene (C_3H_6), cyclopentadiene (C_5H_6), cyclopentene (C_5H_8), fulvene (C_6H_6), and benzene (C_6H_6). Accompanied by electronic structure calculations, the initial JP-10 decomposition *via* C–H bond cleavages resulting in the formation of the initial six $C_{10}H_{15}$ radicals was found to explain the formation of all products detected in both sets of experiments. These radicals are not stable under the experimental conditions and further decompose *via* C–C bond β-scission processes. These pathways result in ring opening in the initial tricyclic carbon skeletons of JP-10. Intermediates accessed after the first β-scission can further isomerize or dissociate. Complex PAH products in the NRLS experiment (naphthalene, acenaphthylene, biphenyl) are likely formed *via* molecular growth reactions at elevated residence times.

1. Introduction

Tricyclo[5.2.1.$0^{2,6}$]decane (*exo*-tetrahydrodicyclopentadiene; *exo*-TCD; Fig. 1) represents a single component hydrocarbon fuel and is the principal constituent of Jet Propellant-10 (JP-10; $C_{10}H_{16}$) as exploited in detonation engines, missiles, and supersonic combustion ramjets. With attractive properties such as high thermal stability, high-energy density, low freezing point, and high energy storage, JP-10 attracts extensive attention[1–39] triggering extensive experimental, theoretical, and modeling investigations to examine the features of oxidative and thermal decomposition mechanisms (Table 1 and Table S1, ESI†).

Green *et al.* presented shock tube experiments combined with kinetic modeling efforts on the pyrolysis and combustion of JP-10.[5] The experiments were performed at 6–8 atm using 2000 ppm of JP-10 over a temperature range of 1000–1600 K for pyrolysis and oxidation equivalence ratios from 0.14 to 1.0. Gas chromatography-mass spectrometry coupled with electron impact ionization (GC-MS-EI) was utilized to identify and quantify the products. They observed that JP-10 decomposed primarily to ethylene (C_2H_4), propene (C_3H_6), cyclopentadiene (C_5H_6), and aromatics such as benzene (C_6H_6) and toluene (C_7H_8), along with trace components like 1,2-divinylcyclohexane ($C_{10}H_{16}$),

[a] *Department of Chemistry, University of Hawaii at Manoa, Honolulu, Hawaii, 96822, USA. E-mail: ralfk@hawaii.edu*
[b] *Chemical Sciences Division, Lawrence Berkeley National Laboratory, Berkeley, California 94720, USA. E-mail: mahmed@lbl.gov*
[c] *Department of Chemistry and Biochemistry, Florida International University, Miami, Florida 33199, USA. E-mail: mebela@fiu.edu*
[d] *National Synchrotron Radiation Laboratory, University of Science and Technology of China, Hefei, 230029, P. R. China*
[e] *Key Laboratory for Power Machinery and Engineering of MOE, Shanghai Jiao Tong University, Shanghai 200240, P. R. China*

† Electronic supplementary information (ESI) available. See DOI: 10.1039/c7cp01571b

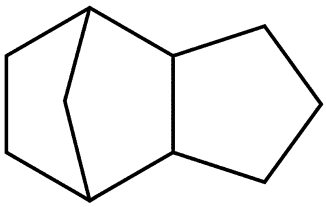

Fig. 1 The molecular structure of JP-10 (*exo*-tetrahydrodicyclopentadiene).

butadiene (C_4H_6), and 1,3-cyclohexadiene (C_6H_8). Anderson *et al.* utilized a small flow tube reactor to investigate the decomposition of JP-10 over the temperature range up to 1700 K on the millisecond time scale.[6] Chemical ionization and electron impact ionization mass spectrometry were utilized to identify the products. They observed that cyclopentadiene (C_5H_6), benzene (C_6H_6), methylacetylene (C_3H_4), and C_4H_x were the principal products in the initial decomposition. At higher temperatures, major products were identified as benzene (C_6H_6), acetylene (C_2H_2), and ethylene (C_2H_4). Reyniers *et al.* performed JP-10 pyrolysis in a continuous flow tubular reactor near atmospheric pressure in the temperature range of 930–1080 K at 1.7 bar, with residence times to be 2.1–9.35 ms.[7] They concluded that polycyclic aromatic hydrocarbon (PAH) formation started from cyclopentadiene (C_5H_6); successive reactions resulted in the formation of naphthalene ($C_{10}H_8$), indene (C_9H_8), and substituted derivatives of bicyclic aromatic compounds. Marquaire *et al.* performed atmospheric thermal decomposition of JP-10 in a jet-stirred reactor at temperatures from 848 to 933 K with residence times between 500 and 6000 ms.[8] They observed eleven products. Major products were hydrogen (H_2), ethylene (C_2H_4), propene (C_3H_6), cyclopentadiene (C_5H_6), benzene (C_6H_6), and toluene (C_7H_8). Rao and Kunzru investigated the product distribution and kinetics of thermal cracking of JP-10 in an annular tubular reactor at atmospheric pressure, in the temperature range of 903–968 K with residence times of 680–6400 ms.[9] The major products were methane (CH_4), ethylene (C_2H_4), propene (C_3H_6), cyclopentene (C_5H_8), cyclopentadiene (C_5H_6), benzene (C_6H_6), and toluene (C_7H_8); rate constants for thermal cracking of JP-10 were determined by non-linear regression analysis to follow $2.4 \times 10^{13} T^{1.1} \exp(-30815.5/T)$, respectively. Striebich and Lawrence explored JP-10 pyrolysis with a high-temperature and pressure flow reactor.[10] The experiment was carried out in the temperature range from 373 K to 873 K at a pressure over 25 atm and residence times between 1 and 5 seconds. This study suggested that the JP-10 pyrolysis products included alkanes, alkenes, cycloalkenes, cyclopentadiene (C_5H_6), and alkylbenzenes. Wohlwend *et al.* experimentally examined the thermal decomposition behavior of high-energy density hydrocarbons under condensed-phase high-temperature conditions from 473 K to 923 K.[11] The pressure was kept at 34 atm with the residence time of 1800 ms at 473 K. They tested several fuels and concluded that JP-10 degradation led to the formation of small amounts of benzene (C_6H_6) and toluene (C_7H_8). Fang *et al.* studied the thermal cracking of JP-10 in a batch reactor under various pressures.[12] The temperature ranged from 823 K to 903 K and the pressure range comprised 1–30 bar. They quantitatively determined the products with GC and GC/MS revealing that with an increase of the pressure, the relative content of ethylene (C_2H_4) or propene (C_3H_6) decreased while those of methane (CH_4), ethane (C_2H_6), and propane (C_3H_8) increased simultaneously. They also found that liquid products including cyclopentane (C_5H_{10}), cyclopentene (C_5H_8), cyclopentadiene (C_5H_6), and *cis*-bicyclo[3.3.0]oct-2-ene (C_8H_{12}) were the major components. Substituted cyclopentene, benzene (C_6H_6), toluene (C_7H_8), and naphthalene ($C_{10}H_8$) were observed at high pressures and temperatures. Later, this group also performed an experimental and kinetic modeling study on the atmospheric pyrolysis of JP-10, iso-octane and JP-10/iso-octane in a stainless-steel tubular reactor at temperatures from 883 K to 963 K.[13] They concluded that the reaction pathway analyses show that the hydrogen abstraction reactions account for more than 80% of the decomposition of JP-10. Bruno *et al.* studied high-pressure JP-10 thermal decomposition in the temperature range from 623 to 698 K.[14] Fifteen products were observed and the decomposition reaction rate constants were determined. Kim *et al.* performed an experimental and molecular modeling investigation on the thermal stability and the primary initiation mechanism of JP-10 in a batch-type reactor.[15] JP-10 was initially decomposed at a temperature of 623 K in their study. 1-Cyclopentylcyclopentene ($C_{10}H_{16}$) and 4-methyl-2,3,4,5,6,7-hexahydro-1*H*-indene ($C_{10}H_{16}$) were the primary decomposition products of JP-10, and C10 hydrocarbons were determined to be the major products. Recently, Liu *et al.* presented an experimental and

Table 1 Compilation of previous experimental studies on the pyrolysis of JP-10

Group	Method	Temperature (K)	Pressure (bar)	Residence time (ms)	Ref.
Green *et al.*	Shock tube	1000–1600	6–8	0.5	5
Anderson *et al.*	Flow tube reactor	298–1700	0.002–0.004	2.10–9.35	6
Reyniers *et al.*	Flow tubular reactor	930–1080	1.7	3.2–5.3	7
Marquaire *et al.*	Jet-stirred reactor	848–933	1	500–6000	8
Kunzru *et al.*	Annular tubular reactor	903–968	1	680–6400	9
Striebich *et al.*	System for thermal diagnostic studies	373–873	34	1038–5000	10
Wohlwend *et al.*	System for thermal diagnostic studies	473–935	34	1800	11
Fang *et al.*	Batch reactor	823–903	1–38	480–26 400	12
Fang *et al.*	Tubular reactor	883–963	1	1.8×10^6	13
Bruno *et al.*	Thermal block	623–698	345	2.4×10^5–7.2×10^7	14
Kim *et al.*	Batch reactor	583–683	40	3.6×10^7	15
Liu *et al.*	Flow reactor	900–1600	0.00667	—	16

kinetic modeling study on JP-10 pyrolysis at low pressure (40 mbar) in the temperature range from 900 K to 1600 K in a flow tube reactor, with synchrotron vacuum ultraviolet photoionization mass spectrometry (SVUV-PIMS) as the diagnostic method.[16] Under their experimental conditions, JP-10 was initially and completely decomposed at 970 K and 1600 K, respectively. Approximately 28 species were identified and quantified in their study, including some major closed-shell molecules and radicals such as molecular hydrogen (H_2), methyl (CH_3), methane (CH_4), acetylene (C_2H_2), ethylene (C_2H_4), ethyl (C_2H_5), propargyl (C_3H_3), allene (C_3H_4), methylacetylene (C_3H_4), allyl (C_3H_5), propene (C_3H_6), vinylacetylene (C_4H_4), 1,3-butadiene (C_4H_6), 1-butene (C_4H_8), cyclopentadienyl (C_5H_5) and cyclopentadiene (C_5H_6).

Besides these experimental investigations, computational chemistry was also exploited to unravel the decomposition mechanism of JP-10. Herbinet *et al.* carried out a kinetic modeling study on JP-10 pyrolysis.[8] They constructed a comprehensive kinetic mechanism with the EXGAS program (used for performing an automatic generation of mechanisms) and the Thergas program (used to calculate thermodynamic data). The kinetic parameters were taken from literature data and estimated from density function theory (DFT) calculations in the case of reactions involving cyclic compounds and diradicals. Reyniers *et al.*[17] developed a detailed kinetic model of JP-10 pyrolysis and refined these data based on rate constant calculations using *ab initio* calculations. Their model predictions agreed well with five independent experimental data sets for JP-10 pyrolysis that cover a wide range of operating conditions without any adjustment of the model parameters eventually updating rate coefficients of the tricyclodecyl radical decomposition reactions *via* a CBS-QB3 calculation. This study revealed further that the decomposition pathways of JP-10 are mainly initiated *via* hydrogen abstraction, and only to a minor amount *via* biradicals generated through carbon–carbon bond rupture processes. Yue *et al.*[18] exploited DFT calculations to compute barrier heights of plausible decomposition pathways of multiple diradicals formed by carbon–carbon bond scission processes of JP-10. Based on the calculations, they proposed possible pathways for diradicals obtained *via* homolytic C–C bond cleavages of JP-10; this project concluded that those diradicals resemble the intermediates of the final products. To elucidate the initial decomposition mechanism, Chenoweth *et al.*[19] carried out molecular dynamic simulations using a reactive force field. This work reported that the decomposition is initiated by carbon–carbon bond scission leading to ethylene (C_2H_2) plus C_8 hydrocarbons or to two C_5 hydrocarbons such as 1,4-pentadiene (C_5H_8) and cyclopentene (C_5H_8). Subsequently, Magoon *et al.*[20] investigated the barrier heights of ring opening processes and intramolecular disproportionation reactions to understand the pyrolysis mechanism of JP-10. Their results provided evidence that the barriers to the disproportionation reactions may be much lower (by up to 32 kJ mol^{-1}) than previously thought in the case of intramolecular disproportionation in a key JP-10 decomposition pathway. Bozzelli *et al.* used density functional theory and the G3MP2B3 (a modified version of the G3MP2 method where the geometries and zero-point vibration energies are taken from B3LYP/6-31G(d) calculations) and CBS-QB3 composite computational methods to evaluate the standard enthalpy of formation of the parent JP-10 molecule and the different tricyclodecyl ($C_{10}H_{15}$) radicals corresponding to loss of a hydrogen atom from the carbon sites.[21] They calculated the enthalpy of formation for JP-10 to be -82 kJ mol^{-1}. Later, they also determined the carbon–carbon bond dissociation energies in JP-10 corresponding to diradical and carbene formation using density functional theory (DFT), and composite methods in conjunction with a series of isodesmic reactions are employed to increase the accuracy in their work.[22] They calculated that the C–C bond dissociation energies (BDEs) range from 324 to 354 kJ mol^{-1} for JP-10 singlet diradical intermediates; C–H BDEs for the parent carbon sites were found to range from 389 to 422 kJ mol^{-1}; and a wider range for C–C BDEs of carbenes from about 322 to 418 kJ mol^{-1} was revealed. Zehe *et al.*[23] studied the thermochemistry of JP-10 employing a variety of quantum chemistry methods, including the Gaussian G*x* and G*x*(MP*x*) (including G2, G2(MP2), G3, G3(MP2), G3(MP2)//B3LYP) composite methods, as well as the CBS-QB3 method, and a variety of isodesmic and homodesmotic reaction schemes, suggesting a heat of formation of -126.4 kJ mol^{-1} at 298.15 K.

However, the summary of the previous studies suggests that an understanding of the unimolecular decomposition of JP-10 (Table 1 and Table S1, ESI†) is incomplete both from the experimental and theoretical viewpoints. Whereas these investigations yielded valuable information on the formation of closed-shell hydrocarbon intermediates and products, these species were mainly analyzed off-line and *ex situ* (GC-MS); however, GC-MS cannot sample radical transient species or thermally labile closed-shell molecules. Recently, Liu *et al.* presented an experimental and kinetic modeling study on JP-10 pyrolysis with SVUV-PIMS as the diagnostic method and detected some unstable intermediates.[16] But with a relatively long residence time, some information for unstable products was still missing. Therefore, the 'molecular inventory' might have been altered since its formation, crucial reaction intermediates cannot be sampled, and detailed information on the reaction mechanisms – the role of radicals and intermediates – cannot always be obtained, but are at best inferred indirectly and qualitatively. Further, excessive pressures facilitate consecutive reactions of the initial decomposition products as evident from the formation of bicyclic PAHs such as naphthalene ($C_{10}H_8$) effectively excluding the elucidation of the initial decomposition products of JP-10. A novel approach requires probing the open- and closed-shell products online and *in situ* without changing the initial 'molecular inventory' from the decomposition and exploiting versatile, non-spectroscopic detection systems so that the complete product spectrum can be sampled quantitatively. These studies will be combined with electronic structure calculations to yield a unified picture on the temperature and pressure dependent decomposition mechanisms of JP-10.

The present investigation represents the combined experimental and theoretical studies to probe the pyrolysis and initial decomposition products of JP-10 ($C_{10}H_{16}$). In this work,

the pyrolysis experiments were explored in two complementary high temperature reactors, in which the decomposition of JP-10 can be probed systematically at combustion-like temperatures. The nascent product distribution – including radicals and thermally labile closed-shell species – are probed on-line and *in situ* in a supersonic molecular beam exploiting soft photoionization with single photon VUV light followed by a mass spectroscopic analysis of the ions in a Re-TOF.[40–57] Two sets of experiments with different residence times of a few 10 μs and of 100 ms were carried out. By limiting the residence time in the reactor to a few tens of microseconds in the first experiment, we aim to probe the initial reaction products excluding successive (higher order) reactions of the initially formed species, which may lead to molecular mass growth processes. By performing a second set of experiments with a much longer residence time at the level of at least 100 ms, we aim to explore interesting phenomena and conclusions on molecular growth and of the stability/decomposition of the initial radical fragments formed in the decomposition of JP-10. Finally, by carrying out molecular beam experiments and combining these studies with electronic structure calculations, we elucidate data on the products, their branching ratios, and reaction mechanisms involved in the decomposition of JP-10 over a broad range of combustion-relevant temperatures and pressures.

2. Experimental methods

2.1. ALS experiments

The first set of the experiments was carried out at the Advanced Light Source (ALS) at the Chemical Dynamics Beamline (9.0.2.) utilizing a chemical reactor (Fig. 2).[40–43,45–49,58] Briefly, the high temperature chemical reactor was a resistively heated silicon carbide (SiC) tube of 20 mm length and 1 mm inner diameter. A gas mixture at a pressure of 600 Torr with 0.03% JP-10 ($C_{10}H_{16}$) (TCI America; >94%) in helium carrier gas (He; Airgas; 99.999%) was prepared by bubbling helium gas through JP-10 kept in a stainless-steel bubbler at 263 ± 1 K. The gas mixture was introduced into the silicon carbide tube at temperatures up to 1600 ± 10 K as monitored by a type-C thermocouple. After exiting the reactor, the molecular beam, which contained the pyrolysis products, passed a skimmer and entered a detection chamber, which housed the Wiley-McLaren Reflectron Time-of-Flight Mass Spectrometer. The products were photoionized in the extraction region of the spectrometer by exploiting quasi-continuous tunable vacuum ultraviolet (VUV) light from the Chemical Dynamics Beamline 9.0.2 of the Advanced Light Source and detected with a microchannel plate (MCP) detector. Here, mass spectra were taken in 0.05 eV intervals from 8.00 eV to 11.50 eV. A set of additional mass spectra was also measured at 15.5 eV to determine hydrogen and methane yields holding ionization energies of 15.5 eV and 12.6 eV, respectively, which cannot be ionized below 11.5 eV. The photoionization efficiency (PIE) curves, which report the intensity of a single mass-to-charge ratio (m/z) *versus* the photon energy, were extracted by integrating the signal collected at a specific m/z selected for the species of interest over the range of photon energies in 0.05 eV increments and normalized to the incident photon flux. The residence time of JP-10 in the reactor tube (20 mm) under our experimental conditions are tens of μs. This would result in typically three to four (1600 K) collisions of a JP-10 molecule with the helium atoms in the reactor at 600 Torr. However, as the pressure drops from 600 Torr to a few Torr at the exit of the reactor, the actual number of collisions is about one on average.[59]

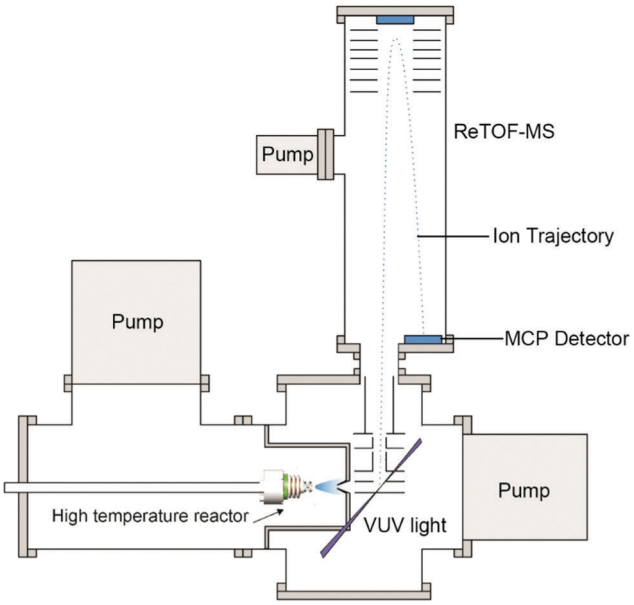

Fig. 2 Schematic experimental setup for ALS experiments.

2.2. NSRL experiments

The second set of experiments was conducted at National Synchrotron Radiation Laboratory (NSRL) in Hefei, China. The detailed description of the apparatus (Fig. 3) can be found in ref. 55 and 60–66. Briefly, the experimental setup consists of three parts: a pyrolysis chamber with a laminar flow reactor heated by a high temperature furnace, a photoionization chamber, and a home-made reflectron time-of-flight mass spectrometer.

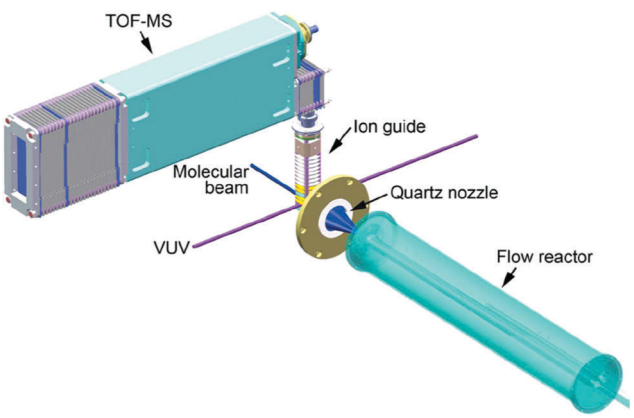

Fig. 3 Schematic experimental setup for NSRL experiments.

The mixture of JP-10 and helium gas was fed into a 0.7 cm inner diameter alumina flow tube with 20.0 cm heated in the high temperature furnace. JP-10 was kept in a stainless-steel bubbler at 266 ± 1 K with a backing pressure of 760 Torr helium. The flow rate of helium was controlled by mass flow controllers (1179A; MKS) at 1000 standard cubic centimeters per minute (SCCM). Thus, the inlet mole fraction of JP-10 was determined to be 0.03%, *i.e.* identical to the experiments at the ALS (2.1). A quartz cone-like nozzle with a 100 μm orifice at the tip was used to sample the pyrolysis species. The sampled pyrolysis species formed a molecular beam and passed into the photoionization chamber, where the neutral molecules are photoionized with tunable vacuum ultraviolet (VUV) light from 8.00 eV to 11.50 eV. A set of additional mass spectra was also measured at 16.64 eV to determine hydrogen and methane. Note that in order to obtain photoionization cross section information of hydrogen, methane, and JP-10 at 16.64 eV, calibration experiments were conducted at 293 K for molecular hydrogen (100 SCCM) and methane (100 SCCM) as well as for JP-10 (266 K) with helium carrier gas (800 SCCM).

Two thermocouples were used for the temperature measurement. A tungsten–rhenium thermocouple was placed close to the center region of the heating wire to monitor the outside temperature of the flow tube, named T_{outside}. A second thermocouple (S-type) was placed inside the flow tube to measure the temperature profiles along the flow tube. The position of the S-type thermocouple can be controlled by a feedthrough outside the pyrolysis chamber. In this work, different T_{outside}s were selected and the temperature profiles along the flow tube were measured. Hence the relationship between T_{outside}s and the temperature profiles inside the flow tube was obtained. Each temperature profile was named according to the maximum temperature measured: T_{max}. The temperature range was selected from 927 K to 1083 K. At 1083 K, JP-10 was almost completely decomposed (<5% left). Thus, no higher-temperature experiment was carried out. The residence time under the selected temperature range and pressure was calculated to be 124–144 ms *via* Chemkin[67] simulations. The temperature profiles are provided in Table S2 in the ESI.†

2.3. Data analysis

PIE analysis[68,69] and branching ratio calculations were performed to reveal their temperature dependence. The detailed methodology is introduced in our previous works.[70,71] Briefly, the PIE curves were fitted by a linear combination of known PIE reference curves from an online PIE database.[72] Since the ion count normalized by the photon fluxes holds a direct proportional relationship with the mole fraction (concentration), the photoionization cross section, mass discrimination ($S_i(T,E) \propto X_i(T)\cdot\sigma_i(E)\cdot D_i$),[50,57,68,69] and the ion counts measured in the experiment, the branching ratios between the concentrations of individual products can be calculated *via* $\left(\frac{X_i(T)}{X_j(T)} = \frac{S_i(T,E)}{S_j(T,E)}\cdot\frac{\sigma_j(E)}{\sigma_i(E)}\cdot\frac{D_j}{D_i}\right)$. The branching ratios of the majority of the products were computed by exploiting photoionization cross sections at 8.0, 8.4, 9.0, 9.5, 10.0, 10.5, 11.0 and 11.5 eV. The data obtained at 15.5 eV (ALS) and 16.64 eV (NSRL) were used to calculate the branching ratios of methane and hydrogen. For the mass discrimination factors, in the ALS experiment, they were taken from ref. 73. In NSRL, the mass discrimination factor fitting is provided in Fig. S1 in the ESI.† The factors are determined to be $\left(\frac{x}{30}\right)^{0.36267}$. It is suggested that uncertainties of experimentally measured photoionization cross sections are 15–20%, while uncertainties of estimated photoionization cross sections are recommended to be 50–200%.[69,74]

3. Computational strategy and methods

A detailed computational study of the complete mechanism of JP-10 pyrolysis is very tricky considering the existence of a great variety of decomposition pathways, extreme complexity of the $C_{10}H_{16}$ potential energy surface (PES) with a large number of possible isomers and transition states, and the presence of multiple primary products, which in turn can undergo secondary decomposition reactions. Therefore, our strategy here is first to identify favorable reaction channels, which may lead to the formation of the most abundant dissociation products observed experimentally. Once such channels are identified, the corresponding regions of the PES are studied in more detail in order to characterize them quantitatively and to generate the energetic and molecular parameters to be used in calculations of rate constants and product branching ratios. Here, the decomposition of a JP-10 molecule can be initiated by a C–C bond cleavage leading to biradical intermediates or by a hydrogen atom loss or abstraction of atomic hydrogen by radicals leading to radical $C_{10}H_{15}$ isomers. A recent theoretical analysis of the reaction pathways by Vandewiele *et al.* has provided evidence that biradical pathways are not expected to play a major role as their overall contribution to the total product yield does not exceed 19%.[7] This result can be attributed to the fact that although C–C bonds in JP-10 are weaker than C–H bonds, additional processes, such as a β-scission-type rupture of another C–C bond or a hydrogen shift followed by a C–C bond cleavage, are required for the initial fragmentation to complete; this results in a higher overall barrier than for a C–H bond cleavage producing a radical fragment in one step. Hence, here we focus on the decomposition pathways of the $C_{10}H_{15}$ radicals R1 to R6 formed by cleavages of various C–H bonds in JP-10. As demonstrated in the present work, these channels occur predominantly *via* β-scission leading to ring opening and/or dissociation but may also involve hydrogen migrations and 'reverse β-scissions', *i.e.* ring closures for which a reverse process is a β-scission.

Geometries of various local minima structures and transition states on the $C_{10}H_{15}$ PES and on the PESs corresponding to decomposition fragments were optimized using the hybrid DFT B3LYP[75,76] method with the 6-311G** basis set and the same method was applied to calculate vibrational frequencies and

zero-point energy (ZPE) corrections. All transition states were tested by animating the motions corresponding to imaginary modes, and in cases where the connectivity of a transition state was not obvious, intrinsic reaction coordinate (IRC) calculations were performed. To refine single-point energies of the optimized structures we applied a modified G3(MP2,CC)//B3LYP[77,78] composite scheme where the energies were computed as

$$E_0[\mathrm{G3(MP2,CC)}] = E[\mathrm{RCCSD(T)/6\text{-}311G^{**}}] + \Delta E_{\mathrm{MP2}} + E(\mathrm{ZPE}),$$

where $\Delta E_{\mathrm{MP2}} = E[\mathrm{MP2/G3large}] - E[\mathrm{MP2/6\text{-}311G^{**}}]$ is a basis set correction and E(ZPE) is the zero-point energy. T1 diagnostics were checked during coupled cluster calculations to ensure that wave functions do not possess any multireference character. The described calculation scheme represents a modification of the original G3[79] method; hereafter, we denote this approach as G3 for brevity. Relative energies computed within this scheme are expected to be accurate within 10 kJ mol^{-1}. All calculations were performed using Gaussian 09[80] and MOLPRO 2010[81] program packages.

4. Experimental results

Fig. 4 and 5 exhibit the mass spectra collected during the pyrolysis of JP-10 ($C_{10}H_{16}$, m/z = 136) at an energy of 10.0 eV at the ALS and NSRL, respectively. Higher harmonic VUV light photoionizes helium, resulting in the peak at m/z = 4 (Fig. 4).

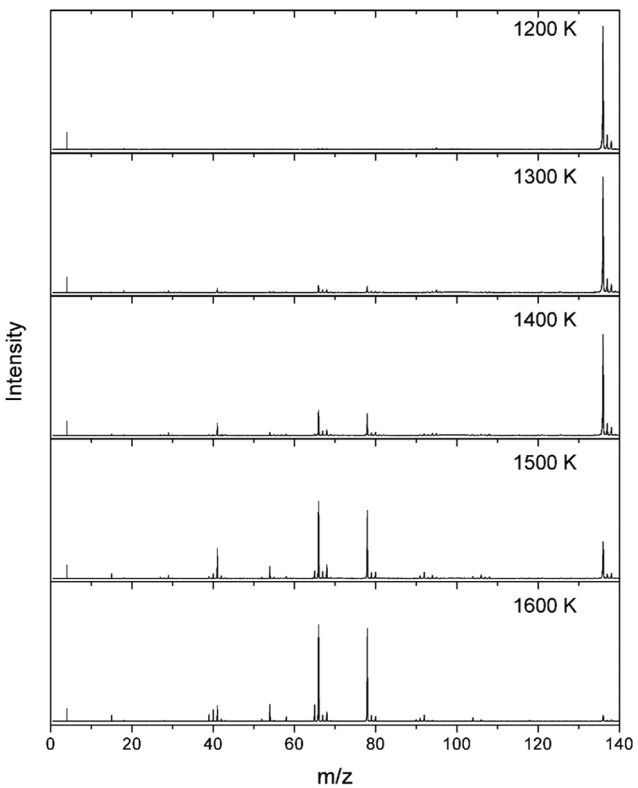

Fig. 4 Mass spectra of the products obtained from the decomposition of JP-10 recorded in ALS at a photon energy of 10.0 eV at different temperatures from 1200 K to 1600 K.

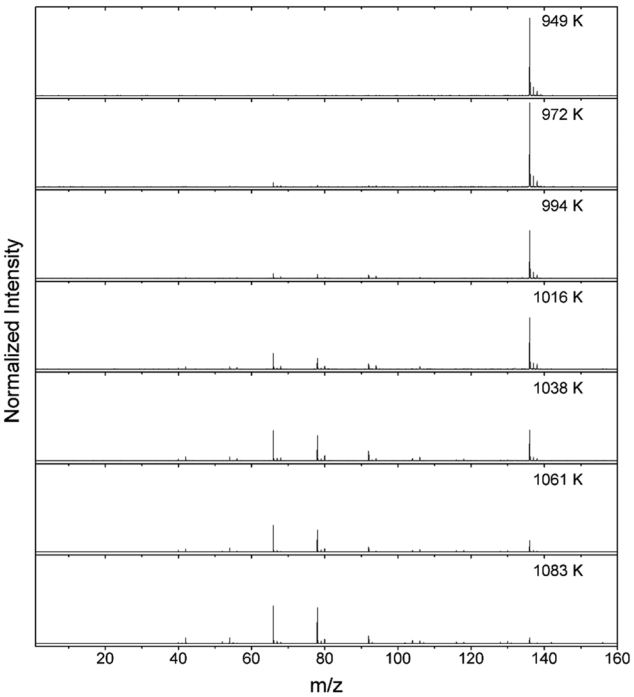

Fig. 5 Mass spectra of the products obtained from the decomposition of JP-10 recorded in NSRL at a photon energy of 10.0 eV at different temperatures from 949 K to 1083 K.

As the concentration of helium is extremely high (>99.9%) but the signal is not very strong, it can be concluded that the photon flux of high-harmonic VUV light can be ignored in the experiment. The photon energy was chosen to be 10.0 eV in Fig. 4 and 5 to avoid the formation of fragment ions from dissociative photoionization of JP-10 at photon energies higher than 10.0 eV. These fragments are labeled as 'JP-10 fragment' in Fig. 6 and 10. Generally, the black lines represent the PIE curve as extracted from the experimental data with the shaded area exhibiting the experimental uncertainties. The red lines are the overall best fit to the PIE curves. If the PIE curves have contributors of more than one species, the blue, green and purple lines are referred to the individual components. The detected mass-to-charge ratios, as well as the chemical formulae and chemical structures of the products, are compiled in Table 2; species observed for the first time in a pyrolysis experiment of JP-10 are emphasized in bold. The photoionization cross sections used for the branching ratio calculation were taken from the online database[72] and individually referenced as listed in Table S3 in the ESI.† Besides, the experimentally determined photoionization energies of the products as extracted from the present study are listed in Table S4 (ESI†).

4.1. ALS results

The mass spectrometric data alone presented in Fig. 4 provide evidence of ion counts of the ionized neutral products from m/z = 15 to m/z = 118 along with the parent ions of the ionized JP-10 precursor at m/z = 136. No ion counts of molecules heavier than JP-10 were observed suggesting that mass growth processes

Table 2 Compilation of products observed in the present experiments on the decomposition of JP-10. Species marked in bold detected for the first time in JP-10 pyrolysis

Molecule	Formula	Mass	Structure	ALS	NSRL
H_2	Hydrogen	2	H–H	+	+
CH_3	Methyl	15	$CH_3^{\bullet}$	+	
CH_4	Methane	16	CH_4		+
C_2H_2	Acetylene	26		+	+
C_2H_3	**Vinyl**	**27**		**+**	
C_2H_4	Ethylene	28		+	+
C_2H_5	Ethyl	29		+	
C_3H_3	Propargyl	39		+	
C_3H_4	Allene	40		+	+
C_3H_4	Methylacetylene	40		+	+
C_3H_5	Allyl	41		+	
C_3H_6	Propene	42		+	+
C_4H_2	Diacetylene	50	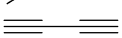	+	
C_4H_4	**1,2,3-Butatriene**	**52**	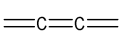	**+**	
C_4H_4	Vinylacetylene	52	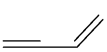	+	+
C_4H_6	1,3-Butadiene	54	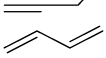	+	+
C_4H_8	1-Butene	56	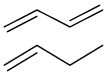	+	+
C_4H_8	2-Butene	56	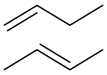	+	+
C_5H_4	**Ethynylallene**	**64**	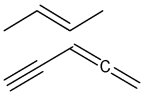	**+**	
C_5H_5	Cyclopentadienyl	65		+	
C_5H_6	Cyclopentadiene	66		+	+
C_5H_8	1,3-Pentadiene	68	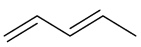	+	+
C_5H_8	Cyclopentene	68		+	+
C_6H_6	Fulvene	78	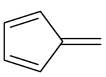	+	+
C_6H_6	Benzene	78		+	+
C_6H_8	1,3-Cyclohexadiene	80		+	+
C_6H_8	1,4-Cyclohexadiene	80		+	
C_6H_{10}	Cyclohexene	82		+	
C_7H_5	**Fulvenallenyl**	**89**	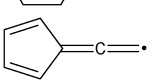	**+**	
C_7H_6	**Fulvenallene**	**90**	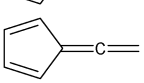	**+**	**+**
C_7H_8	**5-Methylene-1,3-cyclohexadiene**	**92**	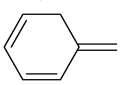	**+**	**+**
C_7H_8	Toluene	92	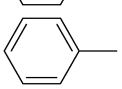	+	+

Table 2 (*continued*)

Molecule	Formula	Mass	Structure	ALS	NSRL
C_8H_6	Phenylacetylene	102	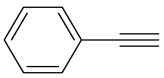	+	+
C_8H_6	Benzocyclobutene	102	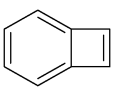	+	+
C_8H_8	***o*-Xylylene**	104	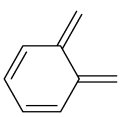	+	+
C_8H_8	Styrene	104	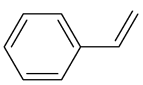	+	+
C_8H_{10}	**1,3,5-Cyclooctatriene**	**106**	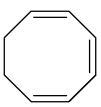	**+**	**+**
C_8H_{10}	*o*-Xylene	106	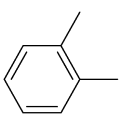	+	+
C_9H_8	Indene	116	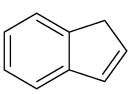	+	+
C_9H_{10}	Indane	118	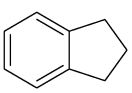	+	+
$C_{10}H_8$	Naphthalene	128	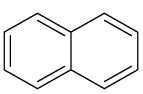		+
$C_{12}H_8$	Acenaphthylene	152	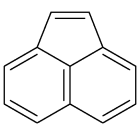		+
$C_{12}H_{10}$	Biphenyl	154	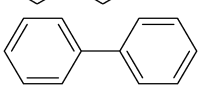		+

to form products heavier than JP-10 are absent. This finding represents a crucial prerequisite for the extraction of the initial pyrolysis products of JP-10. The corresponding photoionization efficiency (PIE) curves along with the best fits are visualized in Fig. 6 at a temperature of 1600 K. The PIE curves at other temperatures and mole fractions of the species observed are provided in the ESI† (Fig. S2 and Table S5). The analysis of the temperature dependence of the PIE curves reveals interesting trends.

First, the intensity of the parent ion of JP-10 (m/z = 136) decreases as the temperature increases from 94% (1200 K) *via* 92% (1300 K), 82% (1400 K) to 32% (1500 K). The precursor is nearly decomposed completely to a level of only 4% at 1600 K (Fig. 7). For the PIE curve of JP-10 at 1600 K, there is redshift for the fitting, meaning there might be isomer(s) of JP-10 not identified in this work.

Second, as compiled in Table 3, as the temperature increases, the number of pyrolysis products increases from seven C1 to C6

species at 1200 K to eighteen (1300 K), twenty-two (1400 K), thirty-three products (1500 K), and thirty-seven C1–C9 products (1600 K). Due to the large number of conceivable isomers for large molecules, there might be some unidentified species generated in this study.

Third, we identified a total of 39 products at different temperatures, which can be arranged into eleven groups. (i) A homologous series of C1–C4 alkenes [ethylene (C_2H_4), propene (C_3H_6), 1-butene (C_4H_8) and 2-butene (C_4H_8)], (ii) dienes [1,3-butadiene (C_4H_6), 1,3-pentadiene (C_5H_8)], (iii) C3–C4 cumulenes [allene (C_3H_4), 1,2,3-butatriene (C_4H_4)], (iv) alkynes [(acetylene (C_2H_2), methylacetylene (C_3H_4))], (v) eneyne [vinylacetylene (C_4H_4)], (vi) diyne [diacetylene (C_4H_2)], (vii) cycloalkenes [cyclopentene (C_5H_8), cyclohexene (C_6H_{10})], (viii) cyclo-dienes [cyclopentadiene (C_5H_6), 1,3-cyclohexadiene (C_6H_8), 1,4-cyclohexadiene (C_6H_8)], (ix) aromatics [benzene (C_6H_6), toluene (C_7H_8), phenylacetylene (C_8H_6), benzocyclobutadiene (C_8H_6), styrene (C_8H_8), *o*-xylene (C_8H_{10}), indene (C_9H_8), indane (C_9H_{10})], (x) radicals [methyl (CH_3), vinyl (C_2H_3), ethyl (C_2H_5), propargyl (C_3H_3), allyl (C_3H_5), cyclopentadienyl (C_5H_5), fulvenallenyl (C_7H_5)], and (xi) some products which could not be grouped to the aforementioned series [hydrogen (H_2), ethynylallene (C_5H_4), fulvene (C_6H_6), fulvenallene (C_7H_6), 5-methylene-1,3-cyclohexadiene (C_7H_8), *o*-xylylene (C_8H_8) and 1,3,5-cyclooctatriene (C_8H_{10})]. Besides, a signal at m/z = 91 was also observed in this work. However, due to excessive photofragments of larger intermediates, the measured PIE curve at m/z = 91 could not be matched with the reference curve of any species holding a mass of 91 amu, not even the benzyl radical. Moreover, signals at m/z = 94 and 108, which should be C_7H_{10} and C_8H_{12}, were also detected in the experiment. However, due to the lack of corresponding PICSs in the database, the products could not be identified or quantified. Therefore, the PIE fittings at m/z = 91, 94 and 108 were not provided in Fig. 6 and Fig. S2 (ESI†), and the corresponding branching ratio could not be calculated. The measured PIE curves of m/z = 91, 94 and 108 are exhibited in Fig. S3–S5 in the ESI.† Besides, some of the products listed above [5-ethenylidene-1,3-cyclopentadiene (C_7H_8, 7.9 eV), benzocyclobutadiene (C_8H_6, 7.5 eV),

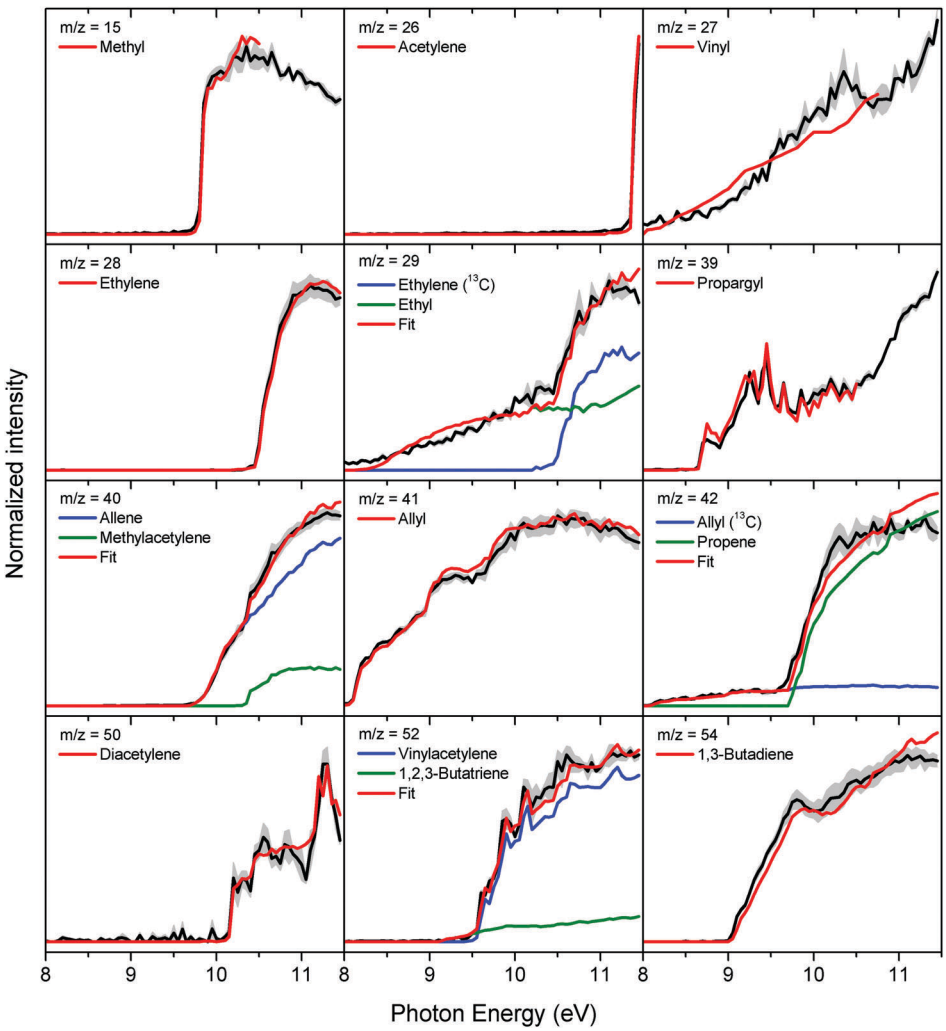

Fig. 6 Experimental photoionization efficiency curves (PIE, black lines) recorded from the decomposition of JP-10 (ALS) at 1600 K along with the experimental errors (gray area) and the reference PIE curves (red, green and blue lines). In the case of multiple contributions to one PIE curve, the red line resembles the overall fit. JP-10 fragment means the photolysis fragment of JP-10.

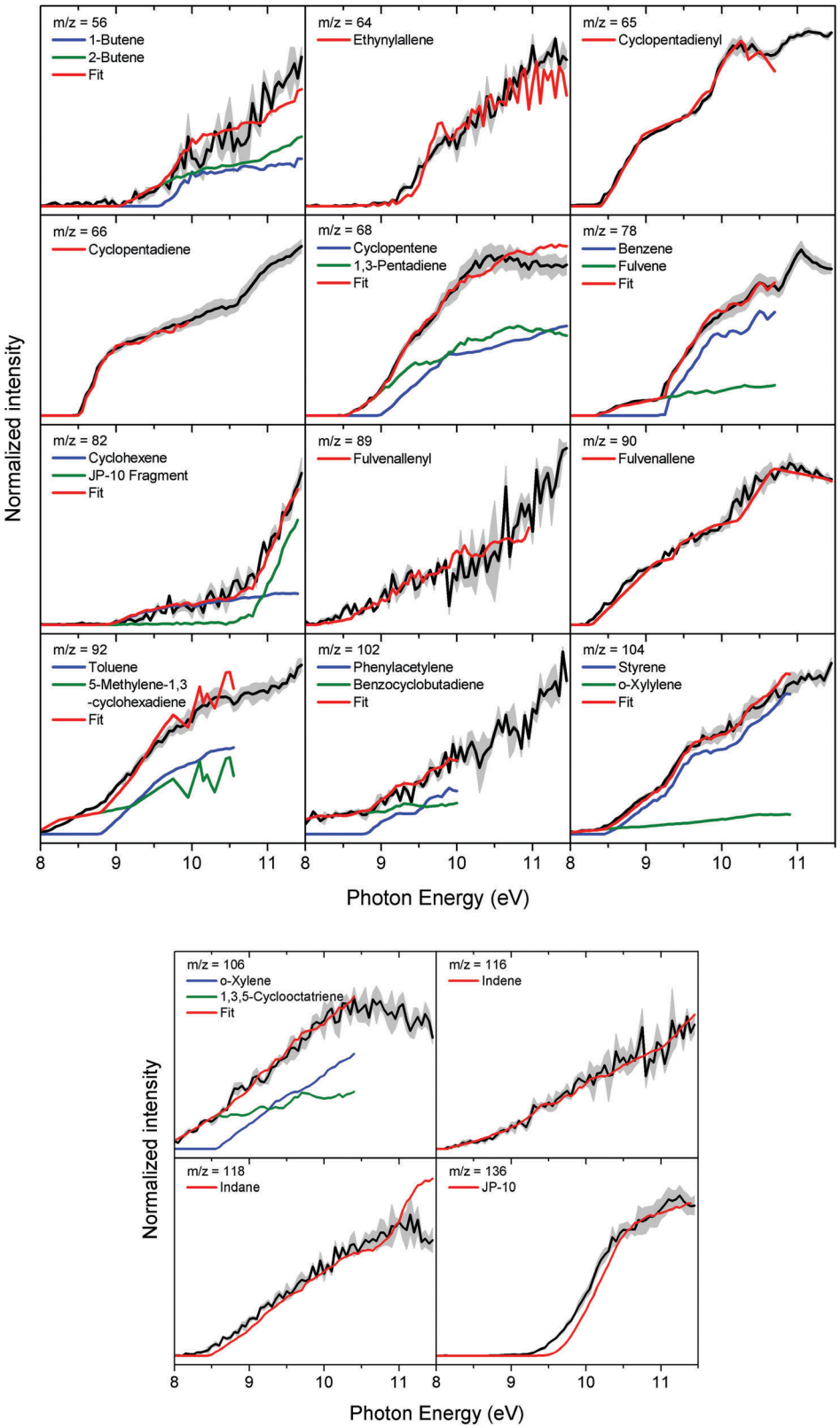

Fig. 6 (cont.)

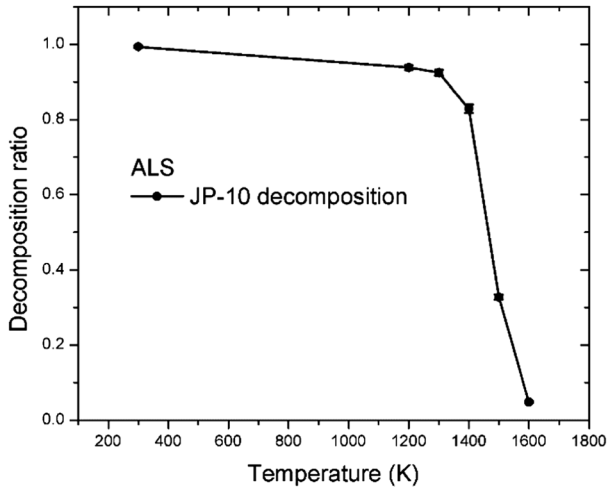

Fig. 7 JP-10 decomposition ratio (ALS) from room temperature to 1600 K.

o-xylylene (C_8H_8, 7.75) and 1,3,5-cyclooctatriene (C_8H_{10}, 7.9 eV)] have photoionization energies below 8.0 eV, which is lower than the experimental energy range. Thus, these species were identified based on the PIE fitting rather than *via* confirming their ionization energy.

Fourth, among these species, it is important to highlight that multiple radicals and thermally labile isomers, *i.e.* vinyl (C_2H_3), 1,2,3-butatriene (C_4H_4), ethynlallene (C_5H_4), cyclopentadienyl (C_5H_5), fulvenallenyl (C_7H_5), fulvenallene (C_7H_6), 5-methylene-1,3-cyclohexadiene (C_7H_8), *o*-xylylene (C_8H_8), and 1,3,5-cyclooctatriene (C_8H_{10}), have been detected for the first time in JP-10 pyrolysis experiments.

Fifth, Table 3 and Fig. 8 quantify that ethylene (C_2H_4) represents the major decomposition products of JP-10 over the complete temperature range increasing from 22% at 1300 K to 27% at 1600 K. The ethyl radical is initially produced at 1200 K, at which temperature ethylene is not yet formed. With increasing temperature, the branching ratio of ethyl decreases significantly from 47%, while that of ethylene keeps increasing. Therefore, we propose that ethylene represents a decomposition product of the ethyl radical. The vinyl radical represents another radical product initially formed at 1300 K. Its decomposition product acetylene increased from 0.2% at 1400 K to 1.85% at 1600 K. The total branching ratio of the C2 species drops from 47% at 1200 K to 30% at 1600 K due to the formation of additional products as discussed below.

Sixth, five C3 species were observed including two radicals and three closed-shell species, which are propargyl (C_3H_3), allene (C_3H_4), methylacetylene (C_3H_4), allyl (C_3H_5), and propene (C_3H_6). Among these products, allyl presents the most dominant product (up to 29% at 1200 K), and it represents one of the initial products in JP-10 pyrolysis formed at 1200 K. As the temperature increases to 1600 K, its overall contribution drops to 5%; however, it remains one of the major products compared with alternate C3 species. The branching ratios of allene and methylacetylene increase from 0.4% (1300 K) to 7.7% (1600 K), indicating that they are also major C3 products. The branching ratios of propene remain below 1% during the entire temperature range illustrating that propene has only a small overall contribution to the JP-10 pyrolysis under the selected conditions.

Seventh, there are six C4 species observed and quantified: diacetylene (C_4H_2), 1,2,3-butatriene (C_4H_4), vinylacetylene (C_4H_4), 1,3-butadiene (C_4H_6), 1-butene (C_4H_8), and 2-butene (C_4H_8). Their production is quite low except for 1,3-butadiene. The latter is formed at 1300 K with a branching ratio of 1.4% and increases to 3.1% with rising temperature. The branching ratios of the other C4 species are below 1%.

Eighth, the cyclopentadienyl radical (C_5H_5) and cyclopentadiene (C_5H_6) are two important C5 species in JP-10 pyrolysis.[7–10,12] Cyclopentadiene appears at 1300 K, while cyclopentadienyl can be seen at 1400 K and above. Both species have high branching ratios at the highest temperature, 5.6% and 18.6%, respectively. This illustrates that they are the major products in JP-10 pyrolysis, which agrees with the conclusion that cyclopentadiene was detected as one of the typical products in previous JP-10 pyrolysis studies. With the advantage of tunable VUV light, the formation of the cyclopentadienyl radical is also revealed. Other C5 species include ethynylallene (C_5H_4), 1,3-pentadiene (C_5H_8), and cyclopentene (C_5H_8). The branching ratio of cyclopentene decreases from 10% at 1200 K to 1% at 1600 K possibly because it represents one of the important reaction intermediates.

Ninth, fulvene (C_6H_6), benzene (C_6H_6), 1,3-cyclohexadiene (C_6H_8), 1,4-cyclohexadiene (C_6H_8), and cyclohexene (C_6H_{10}) constitute the C6 product series in the JP-10 pyrolysis process. Fulvene and cyclohexene are the initial products formed at 1200 K illustrating – based on the temperature dependent branching ratios – that they represent intermediates leading to the formation of small species. With increasing temperature, the branching ratio of fulvene increases from 8.6% at 1200 K to 15.6% at 1400 K, and then drops to 7.2% at 1600 K. Meanwhile, the branching ratio of cyclohexene drops from 4.9% at 1200 K to less than 0.1% at 1600 K. The difference between these two intermediates suggests that fulvene also acts as a major product due to its higher thermal stability. As the temperature increases, the branching ratio of fulvene decreases while the branching ratio of benzene increases simultaneously. It is interesting to note that from 1300 K to 1600 K, the sum of the branching ratios of fulvene and benzene is at the level of 14% to 18% suggesting that fulvene isomerizes to benzene.

Tenth, species larger than C7 are only minor products. Most of these species have branching ratios less than 1%. Four C7 species were observed: fulvenallenyl (C_7H_5), fulvenallene (C_7H_6), 5-methylene-1,3-cyclohexadiene (C_7H_8), and toluene (C_7H_8). Besides, six C8 products and two C9 products were detected as shown in Table 3 and Fig. 6 and Fig. S2 (ESI†). Due to the low production yield, the signal intensities of these species are quite weak leading to relatively high uncertainties. Though very small, 5-methylene-1,3-cyclohexadiene was observed at the initial temperature of 1200 K indicating that this species represents one of the primary intermediates of JP-10 decomposition. Similarly, 1,3,5-cyclooctatriene (C_8H_{10}, m/z = 106) was also observed at 1200 K. For the remaining C7 and C8 species, they are produced

Table 3 Branching fractions (%) of the products in the decomposition of JP-10 at 600 Torr in the chemical reactor (ALS) at 1200, 1300, 1400, 1500, and 1600 K. The numbers in each bracket present the lower and upper uncertainties, respectively

		Temperature				
Molecule	Formula	1200 K	1300 K	1400 K	1500 K	1600 K
Hydrogen	H_2	—	4.26 (−1.26, +1.47)	2.78 (−0.67, +0.72)	2.63 (−0.62, +0.67)	5.90 (−1.35, +1.43)
Methyl	CH_3	—	1.03 (−0.43, +0.54)	1.80 (−0.45, +0.50)	2.73 (−0.61, +0.64)	3.27 (−0.73, +0.77)
Acetylene	C_2H_2	—	—	0.16 (−0.05, +0.06)	0.54 (−0.12, +0.13)	1.86 (−0.39, +0.40)
Vinyl	C_2H_3	—	1.88 (−1.04, +2.27)	0.70 (−0.38, +0.82)	0.38 (−0.20, +0.42)	0.24 (−0.13, +0.27)
Ethylene	C_2H_4	—	22.21 (−5.04, +5.34)	22.48 (−4.85, +5.03)	24.59 (−5.21, +5.35)	27.47 (−5.93, +6.15)
Ethyl	C_2H_5	47.10 (−12.93, +14.69)	12.55 (−2.97, +3.21)	6.93 (−1.55, +1.64)	2.37 (−0.53, +0.55)	0.68 (−0.17, +0.19)
Propargyl	C_3H_3	—	—	—	0.26 (−0.06, +0.07)	0.85 (−0.21, +0.24)
Allene	C_3H_4	—	0.36 (−0.23, +0.31)	0.83 (−0.17, +0.18)	2.50 (−0.60, +0.66)	5.24 (−1.27, +1.38)
Methylacetylene	C_3H_4	—	—	0.17 (−0.05, +0.06)	0.86 (−0.20, +0.22)	2.46 (−0.56, +0.59)
Allyl	C_3H_5	29.02 (−8.47, +9.80)	18.28 (−4.56, +5.02)	17.59 (−4.25, +4.62)	12.95 (−3.11, +3.38)	5.02 (−1.25, +1.37)
Propene	C_3H_6	—	0.76 (−0.24, +0.29)	0.66 (−0.16, +0.17)	0.83 (−0.19, +0.20)	0.93 (−0.21, +0.22)
Diacetylene	C_4H_2	—	—	—	—	0.06 (−0.02, +0.02)
1,2,3-Butatriene	C_4H_4	—	—	—	0.05 (−0.04, +0.10)	0.05 (−0.03, +0.09)
Vinylacetylene	C_4H_4	—	—	—	0.09 (−0.02, +0.02)	0.23 (−0.05, +0.05)
1,3-Butadiene	C_4H_6	—	1.40 (−0.35, +0.38)	1.80 (−0.39, +0.41)	2.49 (−0.53, +0.55)	3.07 (−0.67, +0.69)
1-Butene	C_4H_8	—	—	—	0.09 (−0.03, +0.03)	0.10 (−0.03, +0.04)
2-Butene	C_4H_8	—	—	—	0.03 (−0.01, +0.02)	0.03 (−0.02, +0.02)
Ethynylallene	C_5H_4	—	—	—	—	0.05 (−0.03, +0.05)
Cyclopentadienyl	C_5H_5	—	—	1.43 (−0.75, +1.55)	3.09 (−1.59, +3.27)	5.58 (−2.84, +5.79)
Cyclopentadiene	C_5H_6	—	14.70 (−3.76, +4.18)	18.30 (−4.04, +4.23)	19.91 (−4.39, +4.60)	18.62 (−4.11, +4.30)
1,3-Pentadiene	C_5H_8	—	—	—	0.47 (−0.13, +0.15)	0.64 (−0.15, +0.17)
Cyclopentene	C_5H_8	10.17 (−4.12, +5.16)	5.11 (−1.35, +1.52)	4.19 (−0.88, +0.90)	2.93 (−0.66, +0.70)	1.13 (−0.26, +0.28)
Fulvene	C_6H_6	8.57 (−5.23, +12.35)	14.26 (−8.12, +18.21)	15.54 (−8.14, +17.01)	13.28 (−6.89, +14.28)	7.24 (−3.72, +7.66)
Benzene	C_6H_6	—	1.65 (−0.53, +0.63)	2.83 (−0.68, +0.73)	4.46 (−0.97, +1.01)	7.57 (−1.74, +1.85)
1,3-Cyclohexadiene	C_6H_8	—	—	—	0.20 (−0.04, +0.05)	—
1,4-Cyclohexadiene	C_6H_8	—	—	0.22 (−0.09, +0.12)	0.31 (−0.08, +0.08)	—
Cyclohexene	C_6H_{10}	4.93 (−2.56, +3.35)	0.61 (−0.20, +0.24)	0.26 (−0.10, +0.13)	0.14 (−0.05, +0.06)	0.05 (−0.02, +0.02)
Fulvenallenyl	C_7H_5	—	—	—	—	0.04 (−0.02, +0.05)
Fulvenallene	C_7H_6	—	—	—	0.04 (−0.02, +0.04)	0.21 (−0.11, +0.22)
5-Methylene-1,3-cyclohexadiene	C_7H_8	0.16 (−0.11, +0.29)	0.36 (−0.20, +0.45)	0.45 (−0.24, +0.50)	0.73 (−0.38, +0.80)	0.49 (−0.26, +0.57)
Toluene	C_7H_8	—	0.23 (−0.13, +0.29)	0.35 (−0.18, +0.37)	0.40 (−0.22, +0.46)	0.43 (−0.22, +0.46)
Phenylacetylene	C_8H_6	—	—	—	—	0.01 (−0.00, +0.00)
Benzocyclobutadiene	C_8H_6	—	—	—	—	0.01 (−0.01, +0.02)
o-Xylylene	C_8H_8	—	—	—	0.03 (−0.02, +0.03)	0.03 (−0.01, +0.03)
Styrene	C_8H_8	—	—	—	0.11 (−0.03, +0.03)	0.20 (−0.05, +0.05)
1,3,5-Cyclooctatriene	C_8H_{10}	0.06 (−0.06, +0.17)	0.18 (−0.12, +0.30)	0.22 (−0.12, +0.25)	0.19 (−0.10, +0.21)	0.06 (−0.03, +0.08)
o-Xylene	C_8H_{10}	—	0.17 (−0.07, +0.08)	0.29 (−0.07, +0.08)	0.27 (−0.06, +0.07)	0.09 (−0.02, +0.02)
Indene	C_9H_8	—	—	—	—	0.02 (−0.01, +0.01)
Indane	C_9H_{10}	—	—	—	0.06 (−0.01, +0.02)	0.06 (−0.01, +0.01)

initially at high temperatures suggesting to be the primary decomposition products. The tendencies of their branching ratios *versus* temperature are not obvious due to the low production yields. The heaviest products observed in this work were indane and indene, both of which appear at high temperatures with branching ratios below 0.1%. For indane at 1500 K, the PIE does not present a good fitting. But at 1600 K, the fitting is much better. It might be the low concentration of indane resulting in the unsatisfactory result.

Eleventh, let us evaluate molecular hydrogen and the methyl radical. Molecular hydrogen and the methyl radical were observed as well, but methane could not be detected. In the pyrolysis process, the major formation pathways of molecular hydrogen and methane are similar and proceed *via* hydrogen abstraction and – in the case of methane – also *via* roaming.[82] The absence of methane suggests that roaming processes are absent under our experimental conditions.

Finally, the branching ratios as compiled in Table 3 allow us to determine the overall mass balance of the experiments. The overall carbon-to-hydrogen (C/H) ratio is plotted in Fig. 9 *versus* the temperature. As there are forty species considered (including JP-10), and some of them have no accurate photoionization cross sections, the calculated error bars for the C/H ratio are relatively large. The expected C/H ratio of 0.625 is fully recovered at 1200 K suggesting that the mass balance is conserved. At this initial temperature, seven species were observed, with their photoionization cross sections well defined (ESI†). The precursor is depleted by 6% and most of carbon and hydrogen are still accounted for by JP-10. As the temperature increases, the C/H ratios are slightly higher than the expected ratio of 0.625, but the theoretical value of 0.625 is still covered within the error bars in the entire temperature range.

4.2. NSRL results

The mass spectrometric data reveal evidence of ion counts from m/z = 15 to m/z = 154. Two molecules heavier than JP-10 were observed in the experiment with molecular weights of 152 amu ($C_{12}H_8$) and 154 amu ($C_{12}H_{10}$). The PIE curves along with the

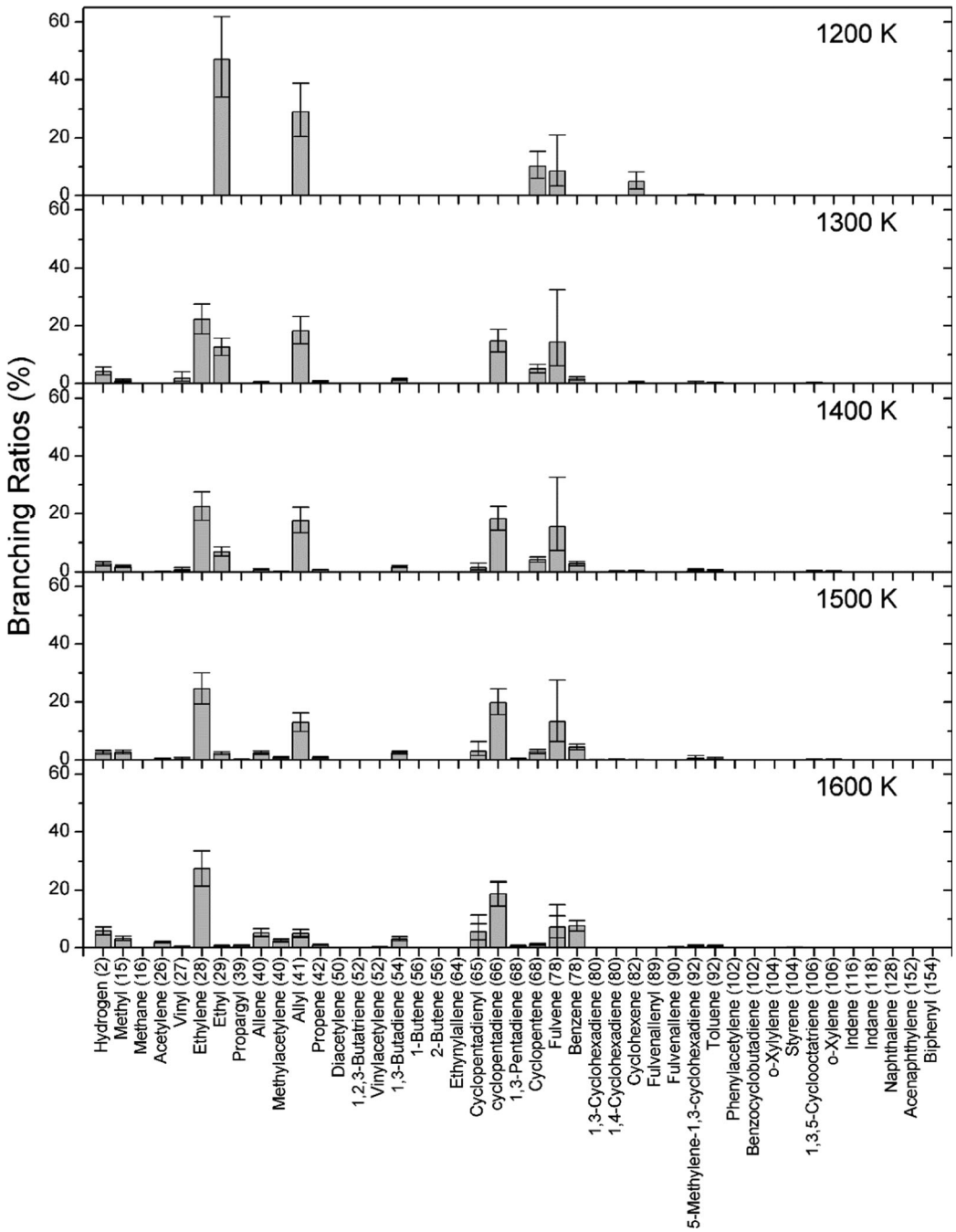

Fig. 8 Overall branching ratios of the species obtained in the decomposition of JP-10 (ALS) in the temperature range from 1200 to 1600 K.

best fits are shown in Fig. 10 for temperature at 1083 K. A detailed analysis of the temperature dependence of the PIE curves reveals the following information. PIE curves at other temperatures are provided in the ESI† (Fig. S6). Mole fractions of the species observed in this experiment are provided in Table S6 in the ESI.†

First, the intensity of the parent ion of JP-10 (m/z = 136) decreases as the temperature increases from 100% (927 K) *via* 95% (949 K), 84% (972 K), 71% (994 K), 54% (1016 K), 29% (1038 K), to 13% (1061 K); the precursor is almost completely decomposed ($<5\%$) at 1083 K (Fig. 11).

Second, as compiled in Table 4, as the temperature increases, the number of pyrolysis products first increases from five C1 to C8 species at 949 K to twelve (972 K), eighteen (994 K), twenty-three (1016 K), twenty-six (1038 K and 1061 K), and thirty C1–C12 products (1083 K). This trend is similar to the ALS data.

Third, 31 products were identified and agreed with most species detected in the ALS experiment with the exception of methane (CH_4), naphthalene ($C_{10}H_8$), acenaphthylene ($C_{12}H_8$), and biphenyl ($C_{12}H_{10}$). Further, the raw data alone suggest that – in strong contrast to the ALS experiments – no radicals were observed. Therefore, we can conclude that a longer residence

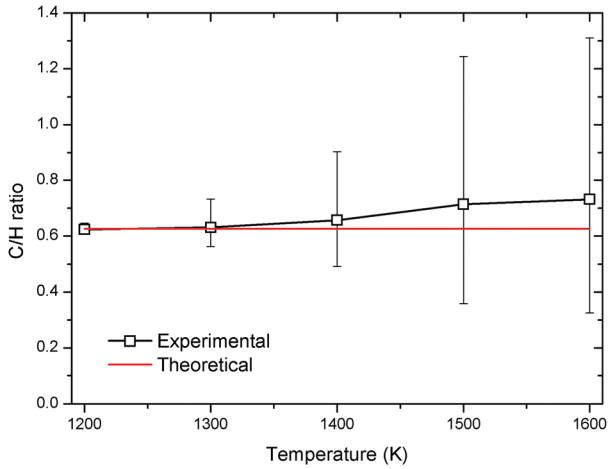

Fig. 9 The C/H ratio of JP-10 pyrolysis (ALS) in the temperature range from 1200 to 1600 K.

time and potentially higher effective pressure in the reactor from a few 10 μs (ALS) to about 100 ms (NSRL) lead either to a decomposition of the radicals or they react to higher molecular weight products. Finally, thermally unstable species, *i.e.* higher energy isomers like 1,2,3-butatriene cannot be detected in the NSRL studies suggesting that they do not survive due to the enhanced residence time in the reactor. Similarly, signals at m/z = 94 and 108 were also detected in the NSRL experiment. The measured PIE curves of m/z = 94 and 108 are exhibited in Fig. S7 and S8 in the ESI.†

Fourth, similar to the ALS experiments, ethylene represents the major product at the NSRL study. Ethylene is formed initially at 949 K and maintains branching ratios above 20% over the entire temperature range. Acetylene represents a second C2 species detected at temperatures over 1016 K. With the temperature increasing, the branching ratio of acetylene increases from less than 1% at 994 K to 2.7% at 1083 K. Smaller species include molecular hydrogen (H_2) and methane (CH_4). Their branching ratios increase as well. For hydrogen, at the highest temperature in this work (1083 K), the branching ratio is 31% contributing with ethylene (23%), cyclopentadiene (16%), and benzene (7%) to a total of 77% of all products.

Fifth, three C3 closed-shell molecules, allene (C_3H_4), methylacetylene (C_3H_4), and propene (C_3H_6), were observed. The appearance temperature for allene and propene is 972 K, and methylacetylene is formed at 994 K. As the temperature increases, the branching ratios of allene and propene drop, while those of methylacetylene increase to branching ratios of 1.4%, 3.9% and 3.4%, respectively. This indicates that allene and propene may act as intermediates in the JP-10 decomposition process. According to previous studies on the isomerization between allene and methylacetylene, there is a tendency for allene to isomerize to methylacetylene;[64,83] the NSRL data support this conclusion. However, the ALS data reveal that the branching ratio of allene is higher than that of methylacetylene over the entire temperature range. This might be because during the short residence time of the ALS experiments, allene is unlikely to isomerize significantly to methylacetylene.

Sixth, comparing the six C4 products detected at the ALS, only four C4 species were observed in NSRL: vinylacetylene (C_4H_4), 1,3-butadiene (C_4H_6), 1-butene (C_4H_8), and 2-butene (C_4H_8). Among these species, 1,3-butadiene possesses the highest branching ratio of 2.2% at 1083 K. It is initially formed at 972 K as 1-butene. As the temperature increases, the branching ratio of 1-butene decreases and reaches 0.3%. Vinylacetylene and 2-butene are only minor products in JP-10 decomposition under the experimental conditions as their branching ratios are lower than 1%.

Seventh, three C5 products were observed, including cyclopentadiene (C_5H_6), cyclopentene (C_5H_8) and 1,3-pentadiene (C_5H_8). Cyclopentadiene and cyclopentene were detected at 949 K suggesting that they represent primary decomposition products of JP-10. With the temperature rising, the branching ratio of cyclopentadiene decreases first, but then increases reaching about 16%. For cyclopentene, the branching ratio increases from 6.7% to 8.6% at temperatures of 949 K and 972 K and then decreases to 0.6% at 1061 K; this species eventually vanishes at 1083 K.

Eighth, for the C6 molecules, fulvene represents one of the primary products, with benzene being monitored as well. Compared to the ALS, with longer residence time of typically 100 ms and potentially higher effective pressure, fulvene is isomerized to benzene more efficiently resulting in a lower concentration of fulvene. Benzene, as a stable aromatic species, contributes a significant carbon flux for the JP-10 decomposition products.

Ninth, 5-methylene-1,3-cyclohexadiene (C_7H_8) exhibits similar characteristics to fulvene; it appears at 949 K as one of the primary products. The branching ratio of the toluene isomer at 1083 K is just 1.3%. But it is higher than the branching ratio of toluene in the ALS experiment of just 0.4%. Further, in the NSRL experiments, identical C8 and C9 species were detected as in the ALS studies. The branching ratios of the C7–C9 aromatics in the NSRL experiments are generally higher (2.6%) than those in ALS experiments (0.8%).

Tenth, with longer residence times, larger PAHs can be synthesized. Compared to the ALS studies, three additional PAHs were observed at the NSRL experiment: naphthalene ($C_{10}H_8$), acenaphthylene ($C_{12}H_8$), and biphenyl ($C_{12}H_{10}$). These products are generated at higher temperatures, especially acenaphthylene and biphenyl. The longer residence time proposed that these PAHs are formed as higher order reaction products with secondary and even higher order reactions.

Eleventh, molecular hydrogen (H_2) and methane (CH_4) were detected in the NSRL experiment with branching ratios of molecular hydrogen higher than those in the ALS experiments. Methane was only observed in the NSRL study.

Finally, the branching ratios as compiled in Table 4 and Fig. 12 allow us to determine the mass balance of the experiments. The overall carbon-to-hydrogen (C/H) ratio is plotted in Fig. 13 *versus* the temperature. The expected C/H ratio of 0.625 is fully reproduced at 949 K suggesting that the mass balance is conserved. As the temperature increases, the C/H ratios are still very close to the expected ratio of 0.625.

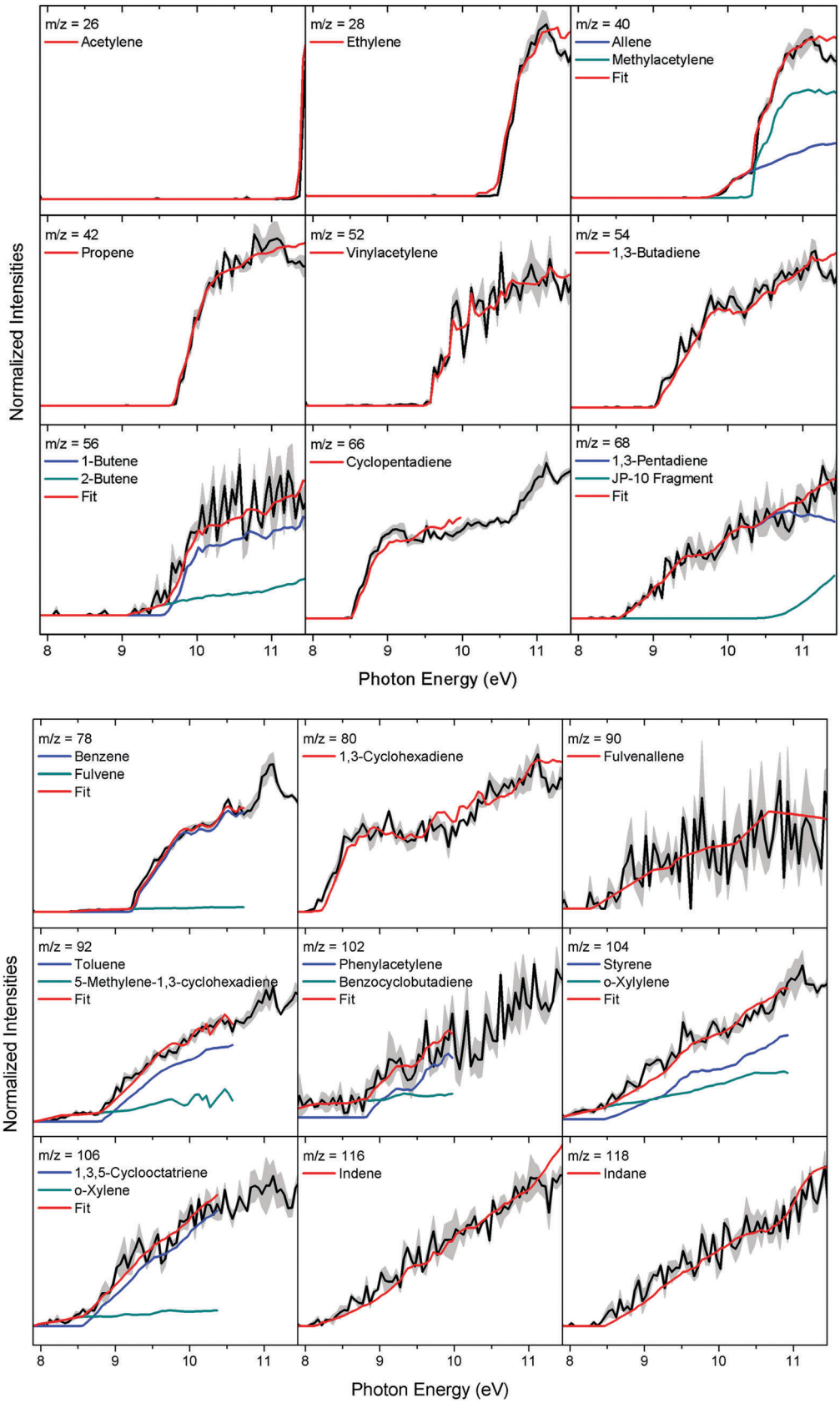

Fig. 10 Experimental photoionization efficiency curves (PIE, black lines) recorded from the decomposition of JP-10 (NSRL) at 1083 K along with the experimental errors (gray area) and the reference PIE curves (blue, green and red lines). In the case of multiple contributions to one PIE curve, the red line resembles the overall fit. JP-10 fragment means the photolysis fragment of JP-10.

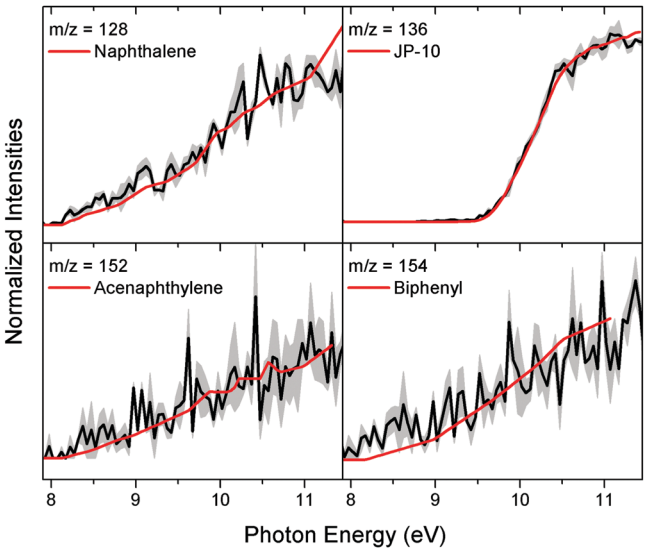

Fig. 10 (cont.)

5. Computational results

5.1. Initial C–H bond cleavages

Fig. 14 illustrates the energetics of various C–H bond cleavages in JP-10 to form the $C_{10}H_{15}$ radicals R1–R6. Based on these energetics, the C–H bond cleavages leading to R1, R4, R5, and R6 are clearly preferable, as they are computed to be endoergic by 397–406 kJ mol^{-1} as compared to 423 and 437 kJ mol^{-1} for the cleavages leading to R3 and R2, respectively. Therefore, hereafter we only consider decomposition processes of the R1 and R4–R6 radicals. All possible initial C–C bond β-scission processes in these radicals are compiled in Fig. 15. These radicals undergo ring opening in the initial tricyclic carbon skeleton of JP-10, but do not lead to a one-step fragmentation. For instance, R1 can isomerize to the radical intermediates R1-1, R1-2, and R1-3 *via* barriers of 150, 106, and 122 kJ mol^{-1}, respectively; R1-1, R1-2, and R1-3 lie 40–52 kJ mol^{-1} higher in energy than R1. R4 exhibits five possible C–C β-scission channels with barriers ranging from 108 to 146 kJ mol^{-1}, and the resulting R4-1–R4-5 intermediates reside 34–73 kJ mol^{-1} above R4. R5 can undergo three possible β-scissions *via* barriers of 97–140 kJ mol^{-1} forming R5-1, R5-2, and R5-3 lying 56–131 kJ mol^{-1} higher in energy than R5. Finally, R6 features only one distinct β-scission pathway producing R6-1 (72 kJ mol^{-1} above R6) over a 141 kJ mol^{-1} barrier. The intermediates accessed after the first β-scission can further isomerize or dissociate giving a variety of JP-10 pyrolysis products. Potential energy diagrams of the dissociation channels including secondary and consequent dissociations of primary products are presented in Fig. 16–22.

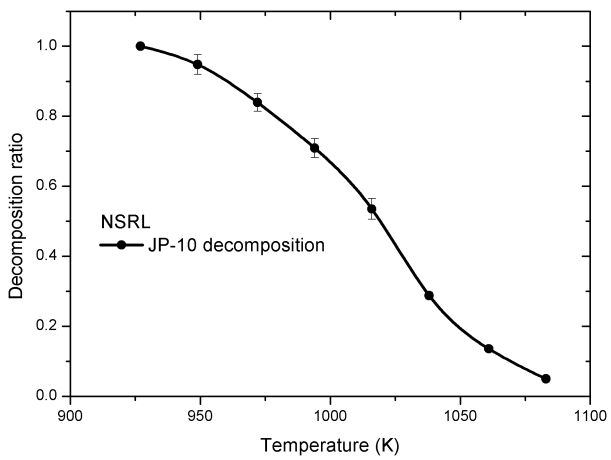

Fig. 11 JP-10 decomposition ratio (NSRL) in the temperature range from 927 to 1083 K.

5.2. The R1 radical

Let us begin with pathways initiated from R1-1 (Fig. 16). A C–C bond β-scission in a five-membered ring of R1-1 leads to the intermediate R1-1_i1 over a 118 kJ mol^{-1} barrier (169 kJ mol^{-1} relative to R1). Yet another β-scission breaks the remaining five-membered ring and produces an open-chain $C_{10}H_{15}$ intermediate R1-1_i2 *via* a barrier of a similar height. Next, R1-1_i2 features a third β-scission step and dissociates to C_4H_6 (1,3-butadiene) + C_6H_9 (R1-1_p1). The last step is rate-determining for the entire pathway from R1 and the corresponding transition state (TS) lies 274 kJ mol^{-1} above the initial reactant. The R1-1_p1 product can in principle further dissociate by β-scission to ethylene (C_2H_4) plus C_4H_5 but the barrier for ethylene loss by β-scission is as high as 157 kJ mol^{-1} and therefore, a reverse β-scission, *i.e.*, a six-membered ring closure to R1-1_p2 (a cyclohexenyl radical; C_6H_9) featuring a barrier of only 45 kJ mol^{-1} should be more favorable. Next, cyclohexenyl can lose a hydrogen atom and produce 1,3-cyclohexadiene (C_6H_8), but this requires overcoming of a significant barrier of 193 kJ mol^{-1}. Alternatively, if the R1-1_p2 product is thermalized in the reactor, it may attach a hydrogen atom *via* a barrierless and highly exothermic reaction to form cyclohexene (C_6H_{10}). The R1-1_p1 product can also be formed

Table 4 Branching fractions (%) of the products in the decomposition of JP-10 at 600 Torr in the flow reactor (NSRL) at 949, 972, 994, 1016, 1038, 1061 and 1083 K. The numbers in each bracket present the lower and upper uncertainties, respectively

		Temperature						
Molecule	Formula	949 K	972 K	994 K	1016 K	1038 K	1061 K	1083 K
Hydrogen	H_2	—	—	29.22 (−22.51, +26.86)	32.78 (−8.74, +9.96)	34.37 (−7.90, +8.90)	33.79 (−8.91, +10.14)	30.76 (−5.03, +5.46)
Methane	CH_4	—	—	—	0.52 (−0.52, +0.62)	1.41 (−0.63, +0.74)	2.56 (−0.68, +0.77)	2.83 (−0.46, +0.50)
Acetylene	C_2H_2	—	—	0.32 (−0.09, +0.11)	0.89 (−0.25, +0.29)	1.14 (−0.35, +0.40)	1.73 (−0.52, +0.61)	2.66 (−0.65, +0.71)
Ethylene	C_2H_4	35.55 (−11.54, +13.75)	32.24 (−10.02, +11.80)	20.64 (−4.63, +4.88)	20.58 (−5.29, +5.88)	20.82 (−4.87, +5.23)	20.04 (−4.42, +4.63)	23.20 (−5.28, +5.60)
Allene	C_3H_4	—	3.12 (−1.14, +1.39)	2.97 (−1.46, +1.89)	2.63 (−1.43, +1.88)	2.44 (−0.66, +0.75)	2.66 (−0.95, +1.16)	1.42 (−0.50, +0.61)
Methylacetylene	C_3H_4	—	—	0.97 (−0.42, +0.53)	1.20 (−0.46, +0.57)	1.50 (−0.39, +0.43)	1.78 (−0.48, +0.55)	3.38 (−0.78, +0.83)
Propene	C_3H_6	—	7.07 (−1.75, +1.92)	5.13 (−1.31, +1.46)	5.23 (−1.28, +1.40)	4.88 (−1.13, +1.21)	4.11 (−0.94, +0.99)	3.89 (−0.91, +0.97)
Vinylacetylene	C_4H_4	—	—	—	0.14 (−0.04, +0.05)	0.16 (−0.04, +0.05)	0.26 (−0.06, +0.07)	0.37 (−0.09, +0.11)
1,3-Butadiene	C_4H_6	—	2.31 (−0.66, +0.76)	1.72 (−0.43, +0.47)	1.96 (−0.51, +0.57)	1.83 (−0.45, +0.49)	1.94 (−0.45, +0.48)	2.22 (−0.49, +0.52)
1-Butene	C_4H_8	—	3.63 (−1.04, +1.20)	3.18 (−0.90, +1.03)	2.48 (−0.57, +0.60)	1.92 (−0.44, +0.46)	0.83 (−0.23, +0.26)	0.29 (−0.08, +0.10)
2-Butene	C_4H_8	—	—	—	—	0.01 (−0.01, +0.01)	0.10 (−0.05, +0.07)	0.07 (−0.05, +0.07)
Cyclopentadiene	C_5H_6	50.58 (−21.77, +27.59)	27.67 (−7.15, +7.96)	16.59 (−3.99, +4.33)	15.41 (−3.72, +4.04)	15.45 (−3.35, +3.48)	16.84 (−4.07, +4.43)	16.49 (−3.87, +4.16)
Cyclopentene	C_5H_8	6.73 (−3.25, +4.19)	8.57 (−2.45, +2.81)	4.10 (−1.37, +1.64)	2.73 (−0.74, +0.84)	1.11 (−0.30, +0.34)	0.63 (−0.21, +0.25)	—
1,3-Pentadiene	C_5H_8	—	—	—	—	0.35 (−0.12, +0.15)	0.18 (−0.06, +0.08)	0.31 (−0.13, +0.16)
Fulvene	C_6H_6	4.67 (−4.17, +12.02)	4.44 (−3.18, +8.28)	5.45 (−3.11, +7.01)	3.04 (−1.73, +3.87)	1.80 (−0.94, +1.97)	1.43 (−0.81, +1.82)	0.75 (−0.45, +1.04)
Benzene	C_6H_6	—	6.01 (−1.78, +2.08)	3.56 (−1.09, +1.27)	4.52 (−1.21, +1.36)	5.62 (−1.52, +1.72)	6.64 (−1.56, +1.68)	7.54 (−1.64, +1.70)
1,3-Cyclohexadiene	C_6H_8	—	—	0.57 (−0.21, +0.25)	0.78 (−0.26, +0.31)	0.95 (−0.28, +0.32)	0.94 (−0.24, +0.26)	0.67 (−0.17, +0.19)
Fulvenallene	C_7H_6	—	—	—	—	—	—	0.02 (−0.01, +0.03)
5-Methylene-1,3-cyclohexadiene	C_7H_8	1.62 (−1.62, +4.85)	2.63 (−1.47, +3.24)	2.24 (−1.20, +2.55)	2.22 (−1.42, +3.44)	1.30 (−0.73, +1.61)	0.82 (−0.45, +0.98)	0.44 (−0.28, +0.68)
Toluene	C_7H_8	—	1.95 (−0.72, +0.89)	1.58 (−0.41, +0.46)	1.38 (−0.41, +0.48)	1.41 (−0.39, +0.45)	1.31 (−0.35, +0.40)	1.35 (−0.33, +0.35)
Benzocyclobutadiene	C_8H_6	—	—	—	—	—	—	0.01 (−0.01, +0.02)
Phenylacetylene	C_8H_6	—	—	—	—	—	—	0.04 (−0.01, +0.01)
o-Xylylene	C_8H_8	—	—	—	0.09 (−0.06, +0.17)	0.04 (−0.03, +0.07)	0.02 (−0.01, +0.04)	0.07 (−0.05, +0.11)
Styrene	C_8H_8	—	—	0.28 (−0.10, +0.13)	0.13 (−0.04, +0.05)	0.29 (−0.07, +0.08)	0.41 (−0.10, +0.11)	0.42 (−0.10, +0.11)
1,3,5-Cyclooctatriene	C_8H_{10}	0.85 (−0.50, +1.15)	0.36 (−0.24, +0.59)	0.34 (−0.19, +0.42)	0.21 (−0.12, +0.25)	0.16 (−0.09, +0.21)	0.07 (−0.04, +0.11)	0.02 (−0.01, +0.02)
o-Xylene	C_8H_{10}	—	—	0.89 (−0.25, +0.29)	0.76 (−0.25, +0.31)	0.70 (−0.18, +0.20)	0.53 (−0.14, +0.15)	0.35 (−0.09, +0.10)
Indene	C_9H_8	—	—	—	0.08 (−0.02, +0.02)	0.10 (−0.03, +0.03)	0.12 (−0.03, +0.03)	0.14 (−0.03, +0.03)
Indane	C_9H_{10}	—	—	0.23 (−0.06, +0.07)	0.22 (−0.07, +0.08)	0.17 (−0.05, +0.05)	0.16 (−0.04, +0.04)	0.11 (−0.03, +0.04)
Naphthalene	$C_{10}H_8$	—	—	—	—	0.06 (−0.02, +0.02)	0.08 (−0.02, +0.02)	0.13 (−0.03, +0.04)
Acenaphthylene	$C_{12}H_8$	—	—	—	—	—	—	0.02 (−0.01, +0.03)
Biphenyl	$C_{12}H_{10}$	—	—	—	—	—	—	0.03 (−0.02, +0.04)

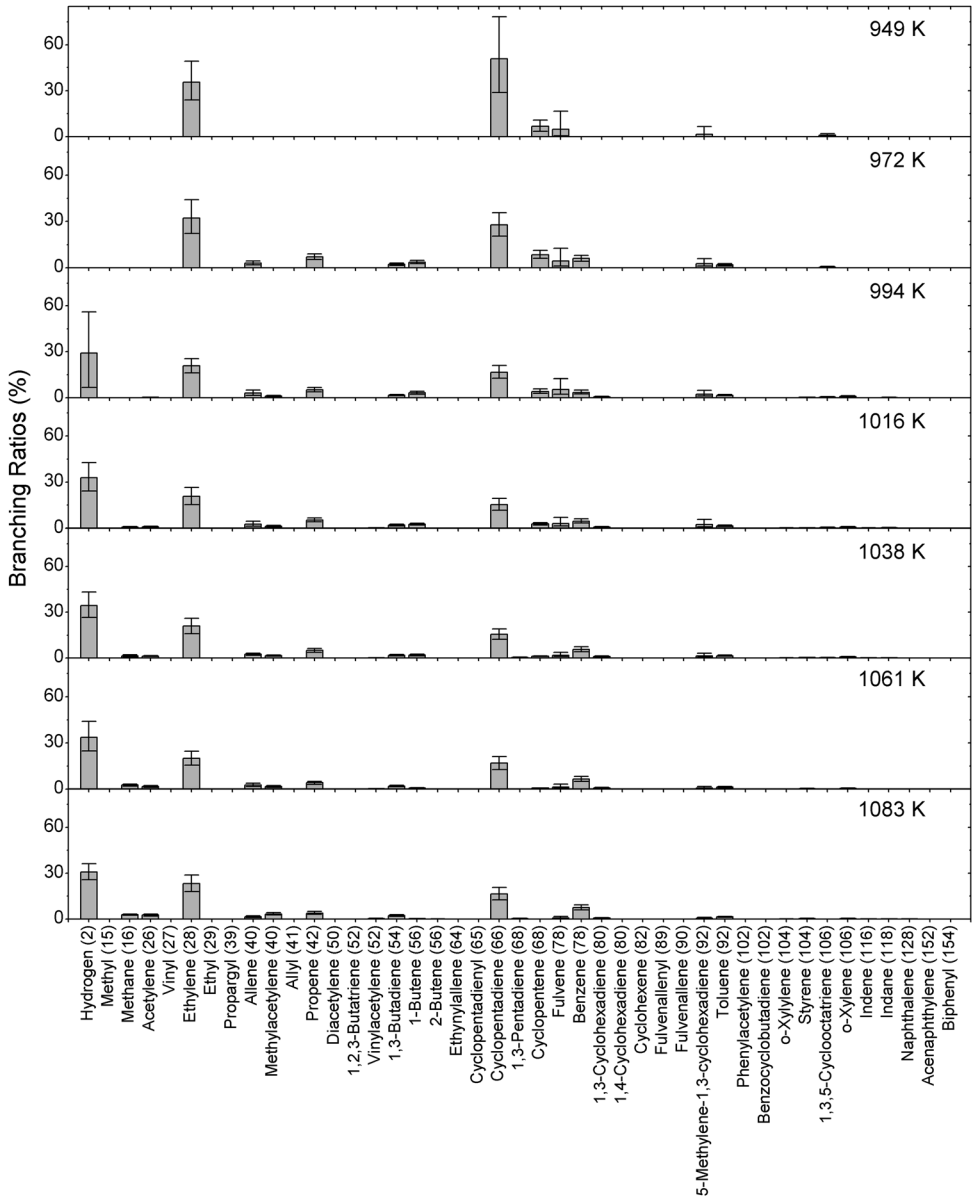

Fig. 12 Overall branching ratios of the species obtained in the decomposition of JP-10 (NSRL) in the temperature range from 949 to 1083 K.

via an alternative pathway involving β-scission of the bond common for the two five-membered rings in R1-1 leading to an eight-membered ring intermediate R1-1_i3. The latter ring opens to the chain structure R1-1_i4, another conformer of R1-1_i2, and then a β-scission process splits C_4H_6 and forms R1-1_p1. However, the critical transition state for C_4H_6 loss on this pathway is higher in energy and resides 331 kJ mol^{-1} above R1. There are other two β-scission reactions in R1-1_i3, vinyl radical (C_2H_3) elimination to R1-1_p4 and ring opening to a branched intermediate R1-1_i5, but both exhibit higher barriers. R1-1_p4 is 1,4-cyclooctadiene (C_8H_{12}) and it may serve as a precursor for 1,3,5-cyclooctatriene (C_8H_{10}) observed experimentally in minor amounts. R1-1_i5 can eliminate the terminal ethylene moiety by β-scission forming a branched C_8H_{11} product R1-1_p5, the fate of which can be threefold. In the most favorable path, R1-1_p5 ring closes to a six-membered ring structure R1-1_p6 overcoming a barrier of only 36 kJ mol^{-1} and the latter can decompose to either 1,4-cyclohexadiene plus vinyl or to 2,5-dihydrostyrene, a precursor of the experimentally observed trace styrene product. Higher-energy and hence much less likely decomposition pathways of R1-1_p5 include terminal acetylene (C_2H_2) elimination forming a branched C_6H_9 structure R1-1_p10, which in turn can fragment to vinyl plus 1,3-butadiene.

The most favorable fragmentation pathway of R1-2 is straightforward (Fig. 17): the bond linking two five-membered rings is cleaved by β-scission leading directly to the cyclopentyl (C_5H_7) plus cyclopentene (C_5H_8) products (R1-2_p1) *via* a barrier of only 168 kJ mol^{-1}. Alternative reaction channels are less competitive. For instance, two different β-scissions in one of the five-membered rings lead to intermediates R1-2_i1 and R1-2_i2

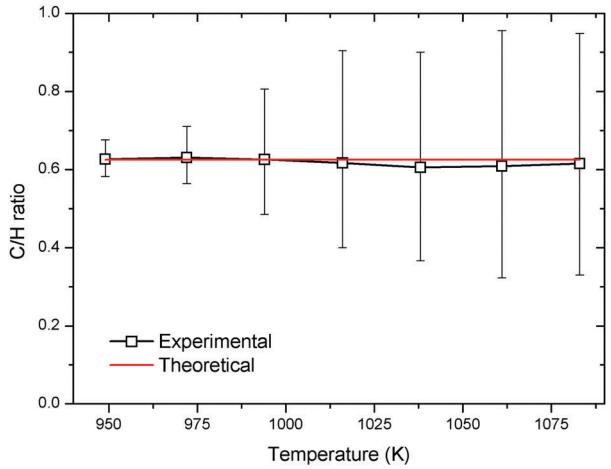

Fig. 13 The C/H ratio of JP-10 pyrolysis (NSRL) in the temperature range from 949 to 1083 K.

via similar barriers of 195–197 kJ mol^{-1} (relative to R1). Next, both intermediates lose ethylene to form the same C_8H_{11} product R1-2_p2, cyclopentene-allyl *via* identical barriers of 217 kJ mol^{-1}. R1-2_p2 can lose an H atom to form C_8H_{10} products R1-2_p4 and R1-2_p5 *via* barriers of 172 and 243 kJ mol^{-1} or, more favorably, undergo a five-membered ring opening followed by a six-membered ring closure leading to the R1-1_p6 product discussed above, a precursor of 1,4-cyclohexadiene and 2,5-dihydrostyrene. The critical transition states for the formation of these products from R1-2_p2 are the vinyl radical and atomic hydrogen loss transition states on the final step residing 184 and 171 kJ mol^{-1} above R1-1_p2. Thus, if some amount of cyclopentene-allyl is produced from R1-2, it is likely to further decompose to the C_8H_{10} isomers R1-2_p4 and R1-1_p7 or to 1,4-cyclohexadiene plus vinyl. The dissociation mechanism of R1-3 is illustrated in Fig. 18. Here it appears that favorable reaction channels involve not only β-scissions but also hydrogen atom migrations. For instance, a 1,2-H shift in R1-3 creating an out-of-ring CH_3 group in the R1-3_i1 intermediate proceeds with a barrier of 199 kJ mol^{-1} relative to R1. Next, R1-3_i1 rearranges to R1-3_i2 by another 1,2-H shift along the six-membered ring *via* a transition state residing 193 kJ mol^{-1} above R1. The primary fragmentation is then completed by β-scission leading to elimination of the methyl group producing a dihydroindane molecule C_9H_{12} (R1-3_p1). In secondary fragmentation channels, dehydrogenation of dihydroindane may lead to indane (C_9H_{10}) and eventually to indene (C_9H_8), both of which were observed in experiments as trace products at high temperatures. Alternatively, following a first hydrogen atom loss from dihydroindane, the reaction may proceed by various β-scissions in C_9H_{11} radicals ultimately resulting in a number of six- and five-membered ring and chain products. A detailed investigation of the decomposition pathways of dihydroindane and related C_9H_{11} radicals will be performed in a separate future work. Alternatively, to the hydrogen atom migration/CH_3 loss pathway, R1-3 can feature two different β-scission processes, both breaking the six-membered ring. The first process leads to the intermediate R1-3_i3 *via* a barrier located 164 kJ mol^{-1} above R1 and then the remaining five-membered ring opens producing a chain R1-3_i4 structure, a conformer of R1-1_i2 and R1-1_i4. Next R1-3_i4 eliminates *trans*-1,3-butadiene producing an open chain C_6H_7 structure R1-3_p2, which is a different conformation of R1-1_p1. Similar to R1-1_p1, R1-3_p2 can ring close and then either eliminate an H atom to form 1,3-cyclohexadiene or add a hydrogen to

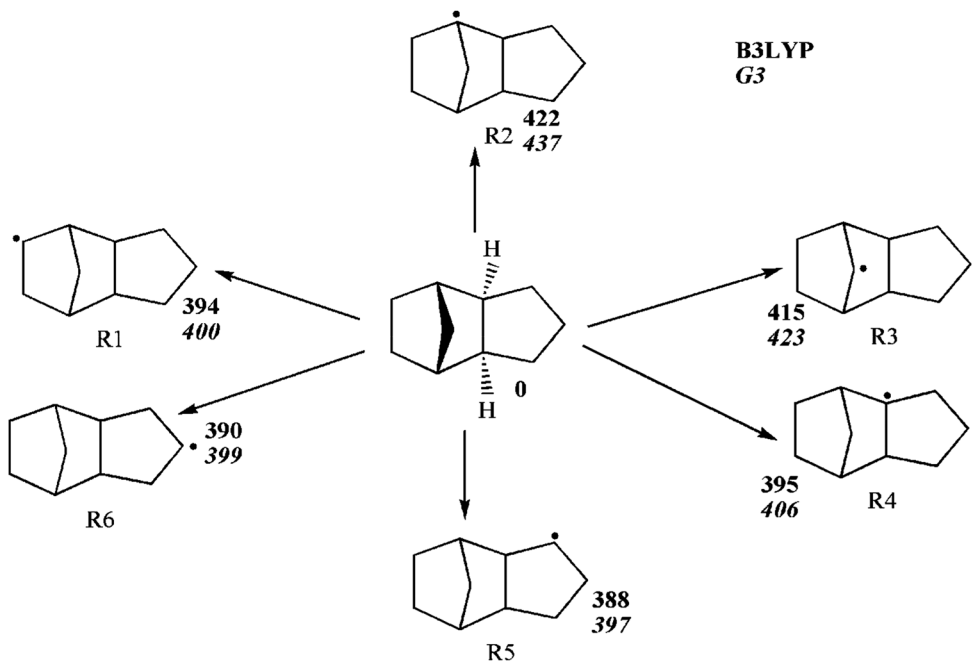

Fig. 14 Radicals formed by C–H bond cleavages in JP-10. Reaction endoergicities calculated at the B3LYP/6-311G** (plain numbers) and G3 levels (italic numbers) are given in kJ mol^{-1}.

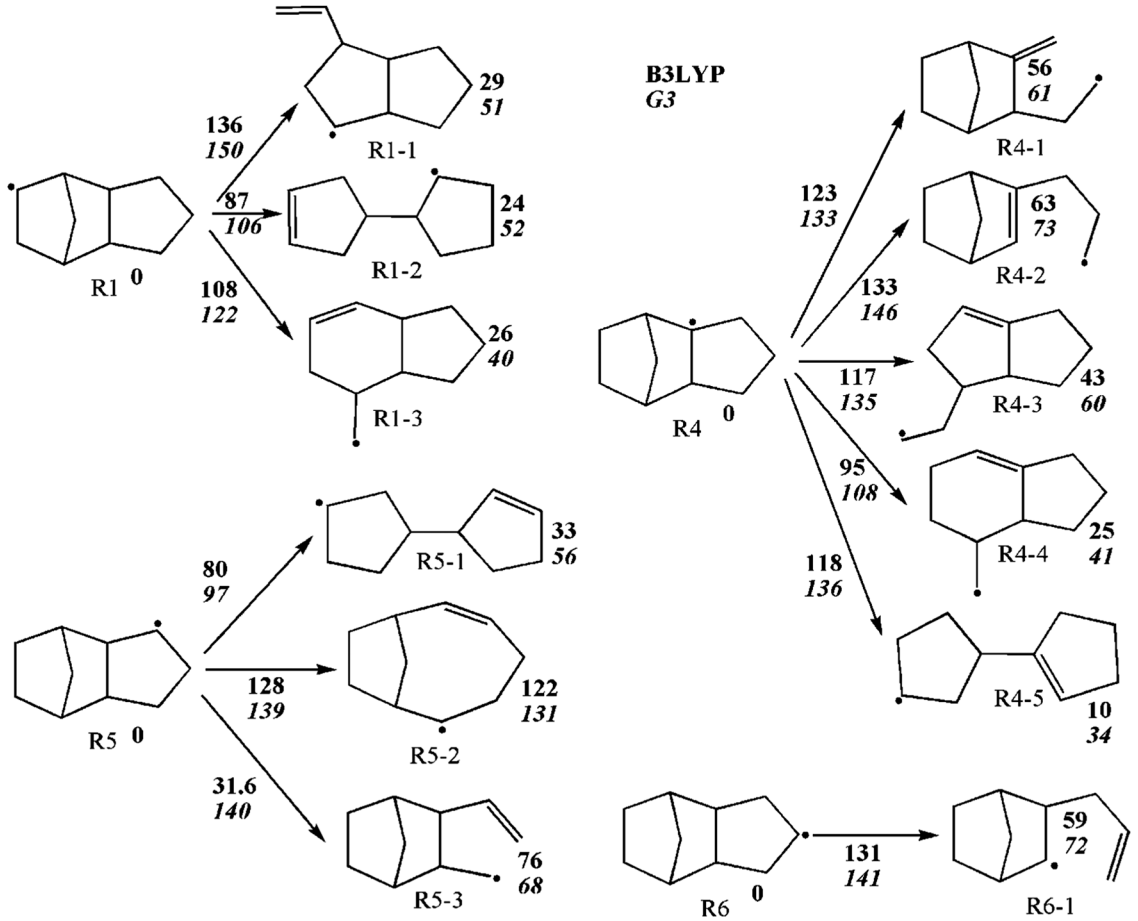

Fig. 15 Energetics of various initial β-scission processes in the R1, R4, R5, and R6 radicals. Relative energies calculated at the B3LYP/6-311G** (plain numbers) and G3 levels (italic numbers) are given in kJ mol^{-1}.

produce cyclohexene. The highest in energy TS on the pathway to C_6H_7 occurs at the last C_4H_6 loss step and resides 274 kJ mol^{-1} above R1. The second β-scission pathway from R3-1 is slightly less favorable. It begins from the formation of R1-3_i5, which next features additional β-scissions making either an open R1-3_i6 or a branched R1-3_i7 intermediate. Both of them eliminate ethylene giving rise to the same C_8H_{11} product R1-3_p3, which can further dissociate to hexatriene plus vinyl or, more favorably, undergo a five-membered ring closure to R1-3_p7 and only then decompose to cyclopentadiene plus an allyl radical. In another channel, R1-3_i5 can dissociate to cyclopentene plus 1,4-pentadien-5-yl, C_5H_7, and the latter can further fragment to allyl (C_3H_5) plus acetylene (C_2H_2), or to serve as a precursor of 1,3-pentadiene observed experimentally.

Summarizing various decomposition channels of R1, R1 → R1-2 → cyclopentene plus cyclopentyl is clearly favored as it features the highest in energy transition at 168 kJ mol^{-1} above R1. This is followed by R1 → R1-3 → R1-3_i1 → R1-3_i2 → R1-3_p1 (dihydroindane plus methyl) (199 kJ mol^{-1}), and then by R1 → R1-1 → R1-1_i1 → R1-1_i2 → R1-1_p1 (C_6H_7 + C_4H_6) (274 kJ mol^{-1}), R1 → R1-3 → R1-3_i3 → R1-3_i4 → R1-3_p2 (C_6H_7 + C_4H_6) (274 kJ mol^{-1}), and R1 → R1-3 → R1-3_i5 → R1-3_p8 (cyclopentene + 1,4-pentadien-5-yl) (274 kJ mol^{-1}). Therefore, dissociation of R1 can largely contribute to the yield of the major five-membered ring products (cyclopentene, cyclopentadiene, cyclopentadienyl) and also provides six-membered rings (cyclohexadienes, cyclohexene, styrene), bicyclic products (indane, indene), as well as smaller molecules and radicals (1,3-butadiene, allyl, ethylene, vinyl radical, acetylene, methyl radical).

5.3. The R4 radical

Next, we consider dissociation of R4 *via* R4-1 and R4-2 (Fig. 19). Two β-scissions in R4 breaking a five-membered ring give similar isomers R4-1 and R4-2, both of which have a common bicyclo core. R4-1 has two side chains, CH_2 and CH_2CH_2, attached to this core, whereas R4-2 has only one $CH_2CH_2CH_2$ side chain. R4-1 and R4-2 fragment by β-scission eliminating ethylene and forming the same C_8H_{11} product R4-1_p1 in which the bicyclo core is maintained. The decomposition channel R4 → R4-1 (R4-2) → C_8H_{11} plus C_2H_4 has a critical barrier of 157 (167) kJ mol^{-1} relative to R4. The primary R4-1_p1 product can further undergo secondary decomposition. The preferable step in the beginning is β-scission breaking the bicyclo core and producing a six-membered ring with two out-of-ring CH_2 groups (R4-1_p2) occurring *via* a barrier of 148 kJ mol^{-1}. Then it appears that a multi-step

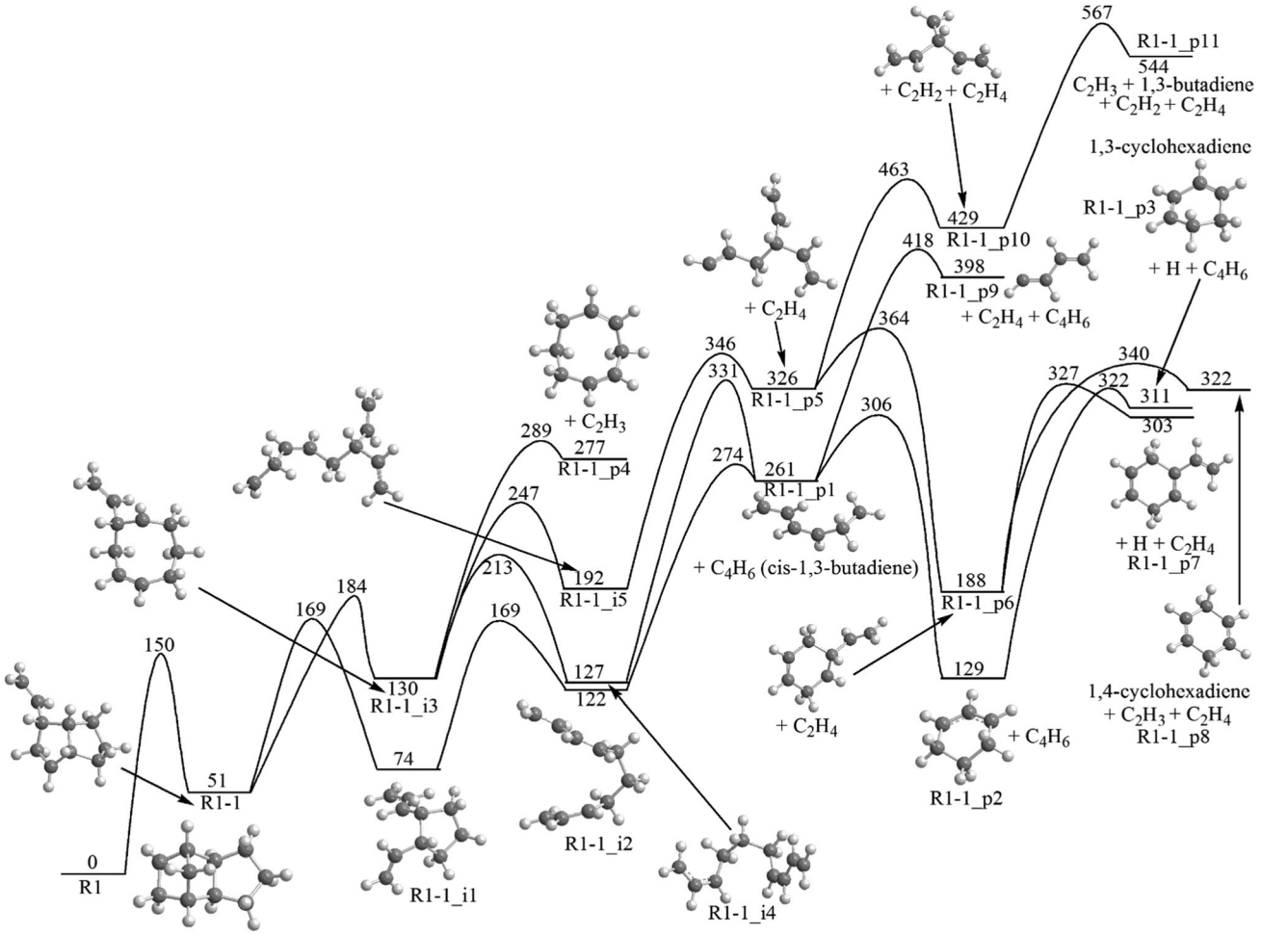

Fig. 16 Potential energy diagram for decomposition of R1-1. All relative energies are computed at the G3 level and are given in kJ mol^{-1}.

process involving a series of 1,2-H shifts is more energetically favorable than another β-scission in R4-1_p2 followed by fragmentation. The hydrogen migration sequence, R4-1_p2 → R4-1_p3 → R4-1_p4 → R4-1_p5 → R4-1_p6, has the highest barrier of 212 kJ mol^{-1} relative to the initial C_8H_{11} radical R4-1_p1. The alternative β-scission sequence R4-1_p2 → R4-1_p11 → C_6H_7 (R4-1_p12) plus C_2H_4 features a much higher barrier of 301 kJ mol^{-1} relative to R4-1_p1. The C_8H_{11} intermediate R4-1_p6 can lose a hydrogen forming *o*-xylene or be subjected to two additional 1,2-H shifts, R4-1_p6 → R4-1_p7 → R4-1_p8, and then eliminate a methyl group and form toluene. Here, the R4-1_p7 and R4-1_p8 intermediates can also dissociate to *o*-xylene plus hydrogen. If some amount of the R4-1_p12 (C_6H_7) product is formed, it can either dissociate to a C_4H_5 radical and acetylene *via* a barrier of 163 kJ mol^{-1} or more likely feature a five-membered ring closure to R4-1_p13 *via* a barrier of only 48 kJ mol^{-1}. The C_6H_7 radical R4-1_p13 is a well-known precursor of fulvene and benzene. Whereas the dissociation of R4-1_p13 predominantly produces fulvene, hydrogen atom-assisted isomerization of fulvene to benzene is fast under combustion conditions. Among other products, the C_4H_5 radical formed here can serve as a precursor of both vinylacetylene and 1,2,3-butatriene observed in the present experiments at high temperature.

Decomposition of the R4-3 intermediate can account for the prompt formation of the ethyl (C_2H_5) radical, which shows the highest branching ratio of all products at the lowest ALS experimental temperature of 1200 K. As seen in Fig. 20, a 1,4-H shift to the terminal CH_2 group of the side chain in R4-3 requires a relatively low barrier of 70 kJ mol^{-1} (144 kJ mol^{-1} with respect to R4) and leads to the R4-3_i1 intermediate. A β-scission in the latter forms the C_8H_{10} (R4-3_p1) plus ethyl radical products after overcoming a barrier lying 154 kJ mol^{-1} higher in energy than R4. Alternatively, ethylene elimination from R4-3 proceeds *via* a barrier of 103 kJ mol^{-1} (177 kJ mol^{-1} with respect to R4) and forms a C_8H_{11} product R4-3_p2. Secondary decomposition of R4-3_p2 should be rather facile as it proceeds by two consecutive β-scissions (five-membered ring opening followed by ethylene elimination) *via* the highest barrier of 130 kJ mol^{-1} relative to the C_8H_{11} reactant R4-3_p2. This decomposition produces C_6H_7, R4-1_p13, a precursor of fulvene and benzene. Secondary decomposition of the closed-shell C_8H_{10} product R4-3_p1 requires further investigation, but it is probable that after activation of R4-3_p1 by a C–H bond cleavage, a C_8H_9 radical would decompose to fulvene plus vinyl also contributing to the yield of C_6H_6 species. The most favorable pathway of R4-4 decomposition, R4-4 → R4-4_i1 → R4-4_i2 → R4-4_p1 plus methyl,

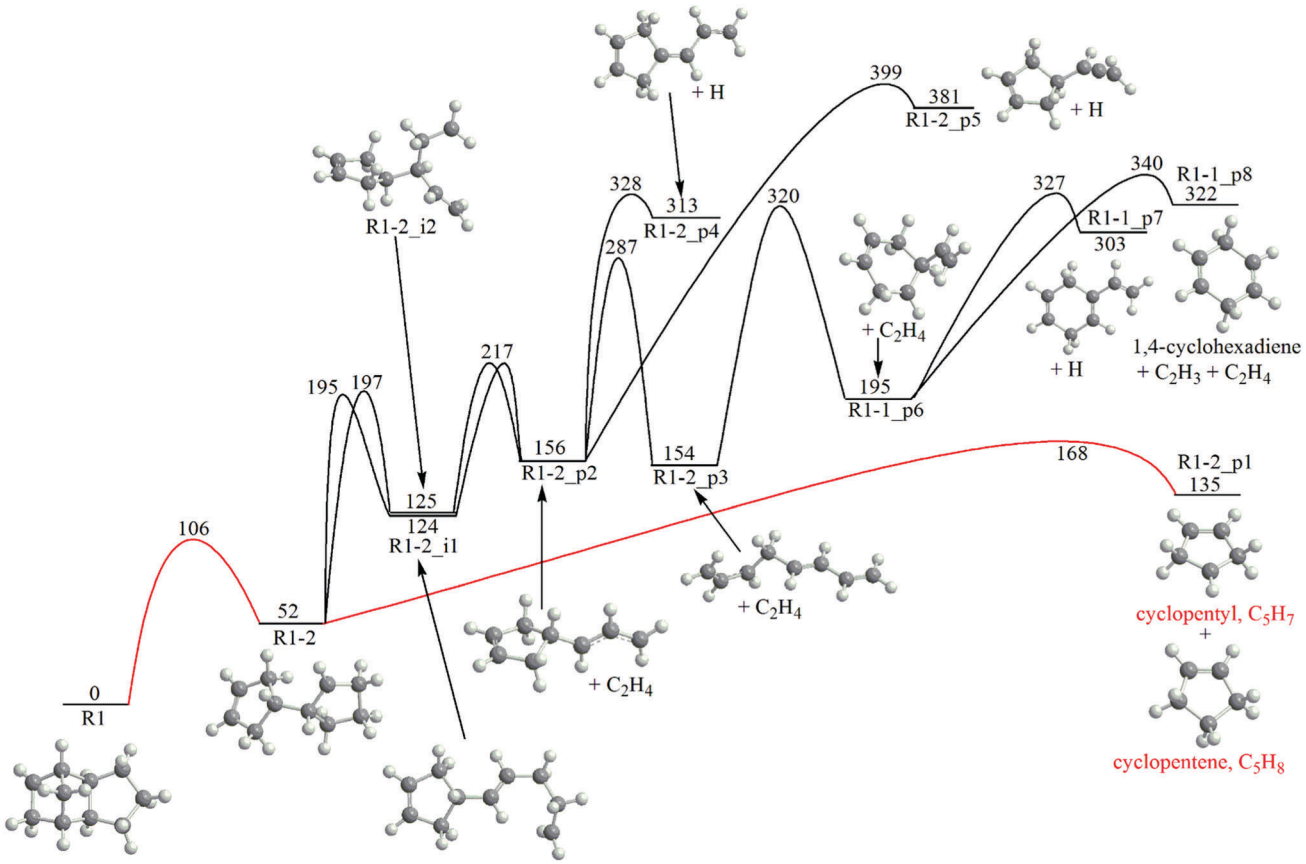

Fig. 17 Potential energy diagram for decomposition of R1-2. All relative energies are computed at the G3 level and are given in kJ mol^{-1}. The red lines and products are preferred.

consists of two 1,2-H shifts followed by elimination of the methyl group (Fig. 20). The highest barrier along this reaction channel is 188 kJ mol^{-1} with respect to R4. The bicyclic C6–C5 core is conserved and the R4-4_p1 product is dihydroindane, a precursor of indane, indene, or other fragments containing either a six- or a five-membered ring, similarly to its R1-3_p1 isomer considered above. In contrast to R4-4, R4-5 prefers to fragment *via* two consecutive β-scissions, R4-5 → R4-5_i1 → R4-5_p1 plus allyl. The critical barrier on this pathway, 195 kJ mol^{-1}, is slightly higher than that for the decomposition of R4-4. The R4-5_p1 product C_7H_{10} is 1-vinyl-1-cyclopentene. It may serve as a precursor of the observed trace products fulvenallene, C_7H_6, and fulvenallenyl, C_7H_5; however, a large number of dehydrogenation steps are required to form those species. If R4-5_p1 is activated by hydrogen atom abstraction or a C–H bond cleavage, the C_7H_9 radicals produced are likely to decompose through β-scissions, but a detailed mechanism requires further investigations.

In summary, the fragmentation pathways of R4 can be ranked in terms of their kinetic favorability based on the height of the highest barrier (given in parentheses relative to R4) as follows: (1) R4 → R4-3 → R4-3_i1 → C_8H_{10} (R4-3_p1) + C_2H_5 (154 kJ mol^{-1}), (2) R4 → R4-1 → C_8H_{11} (R4-1_p1) + C_2H_4 (157 kJ mol^{-1}), (3) R4 → R4-3 → C_8H_{11} (R4-3_p2) + C_2H_4 (177 kJ mol^{-1}), (4) R4 → R4-4 → R4-4_i1 → R4-4_i2 → C_9H_{12} (R4-4_p1) + CH_3 (188 kJ mol^{-1}), and (5) R4 → R4-5 → R4-5_i1 → C_7H_{10} (1-vinyl-1-cyclopentene, R4-5_p1) + C_3H_5 (195 kJ mol^{-1}). Therefore, decomposition of R4 represents a source of the methyl, ethyl, and allyl radicals, ethylene, fulvene and benzene (*via* secondary decomposition of R4-3_p1 and R4-3_p2), and also provides feasible pathways to the minor products *o*-xylene and toluene (*via* secondary dissociation of R4-1_p1), indane and indene (from R4-4_p1), as well as fulvenallene and fulvenallenyl (R4-5_p1).

5.4. The R5 radical

Decomposition of R5 appeared to favorably proceed *via* R5-1 rather than R5-2 or R5-3 and hence Fig. 21 shows only pathways involving R5-1. Here, R5-1 can be subjected to two different β-scissions breaking a five-membered ring *via* similar barriers of 193 and 200 kJ mol^{-1} and forming the R5-1_i1 and R5-1_i2 intermediates. Both intermediates can decompose by eliminating allyl and forming the C_7H_{10} product 3-vinyl-1-cyclopentene R5-1_p1. Alternatively, R5-1_i2 can also dissociate to cyclopentyl (C_5H_7) plus 1,4-pentadiene (R5-1_p2). The critical barriers for the product formation from R5 are found to be in a narrow range of 217–222 kJ mol^{-1}. An alternative pathway from R5-1_i1 to an open-chain structure R5-1_i3 followed by ethylene elimination is unlikely to be competitive because of a much higher critical barrier of 344 kJ mol^{-1} with respect to R5. Thus, decomposition of R5 is a source of the cyclic and open chain C5

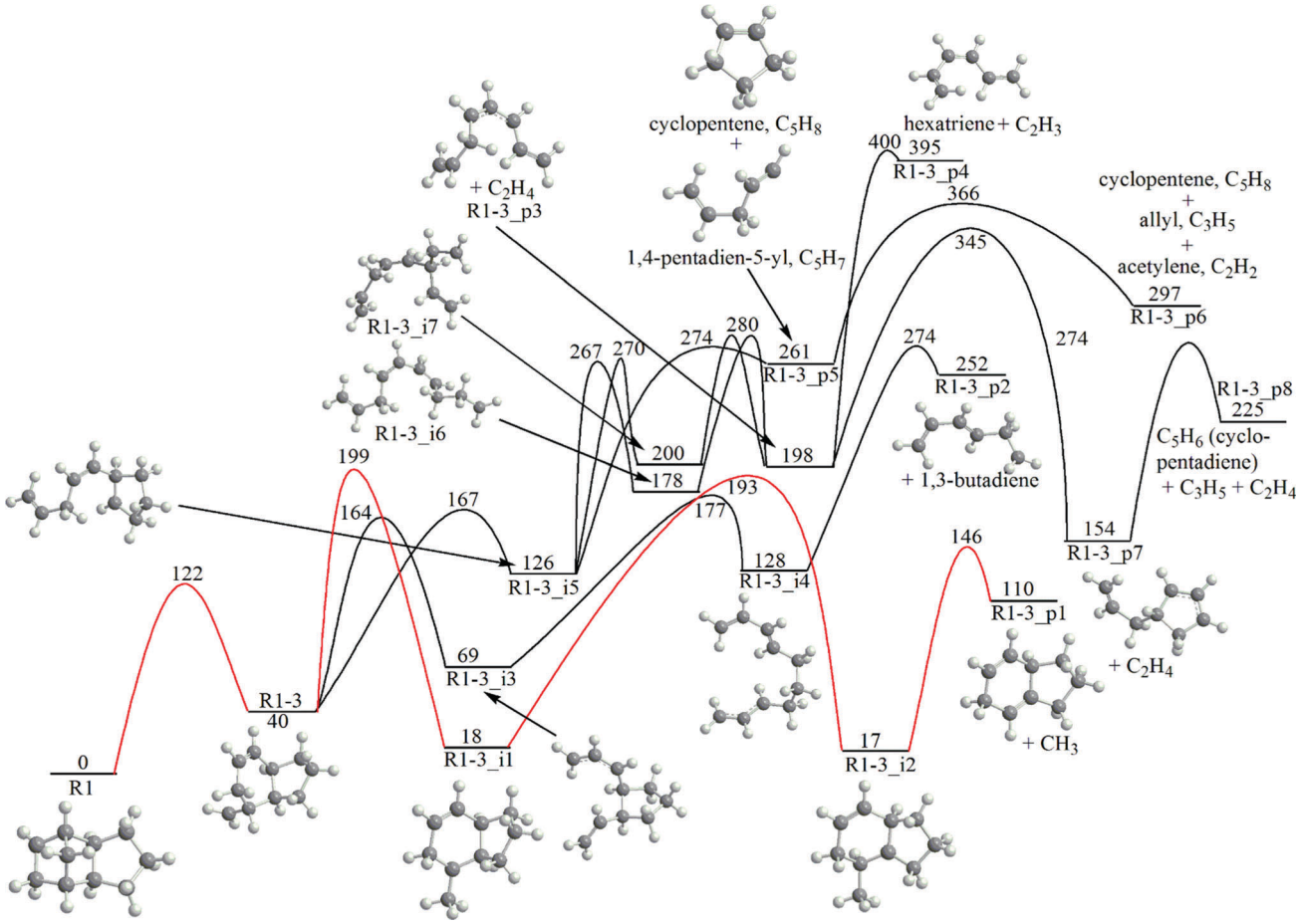

Fig. 18 Potential energy diagram for decomposition of R1-3. All relative energies are computed at the G3 level and are given in kJ mol^{-1}. The red lines are preferred.

fragments and may also contribute to the formation of the trace fulvenallene and fulvenallenyl products through dehydrogenation of 3-vinyl-1-cyclopentene R5-1_p1. Due to the higher barriers, the primary decomposition of R5 is expected to be somewhat slower than that of R1 and R4.

5.5. The R6 radical

Two channels may compete in dissociation of R6 proceeding *via* R6-1 (Fig. 22). In the first one, R6-1 decomposes to the bicyclic C_7H_{10} structure R6-1_p1 plus allyl *via* a barrier of 177 kJ mol^{-1} relative to R6. In the second channel, a first β-scission in R6-1 breaks a five-membered ring and forms the R6-1_i1 intermediate and a second β-scission eliminates ethylene leading to the C_8H_{11} product R6-1_p2, with the highest in energy transition state lying 231 kJ mol^{-1} above R6. The R6-1_p2 product can then easily dissociate to cyclopentadiene (C_5H_6) plus allyl (C_3H_5) overcoming a barrier of only 87 kJ mol^{-1}. Since the C_7H_{10} product R6-1_p1 was not observed in the present experiments, it is likely to undergo further fragmentation in the reactor. While a more detailed study is needed to consider all possible decomposition pathways of R6-1_p1, here we consider only one of them, initiated by the cleavage of one of the C–H bonds leading to the C_7H_9 radical R6-1_p4. The strength of this C–H bond (endoergicity of R6-1_p1 → R6-1_p4 + H) is computed to be 401 kJ mol^{-1}, very similar to the analogous C–H bond strength in JP-10, JP-10 → R1 + H. R6-1_p4 can decompose *via* two competitive mechanisms involving β-scissions. The R6-1_p4 → R6-1_p5 → 5-methylene-1,3-cyclohexadiene (R6-1_p6) plus atomic hydrogen sequence involves reformation of the bicyclic structure into a six-membered ring with an out-of-ring CH_2 followed by H elimination. The highest barrier on this reaction pathway is 136 kJ mol^{-1} relative to the initial C_7H_9 radical R6-1_p4. This channel can account for the observation of a minor 5-methylene-1,3-cyclohexadiene product. Alternatively, the R6-1_p4 → R6-1_p7 → C_5H_6 + C_2H_3 sequence first produces a five-membered ring intermediate with an outer vinyl group and the intermediate then decomposes to cyclopentadiene plus vinyl *via* a barrier of 155 kJ mol^{-1}. In summary, decomposition of R6 contributes to the production of an allyl radical, ethylene, cyclopentadiene (both directly and *via* dissociation of the primary C_7H_{10} R6-1_p1 product), as well as a vinyl radical and 5-methylene-1,3-cyclohexadiene both of which can be formed *via* R6-1_p1.

6. Discussion & conclusions

The calculated PESs and reaction mechanisms deduced allow us to qualitatively account for all observed products of JP-10 pyrolysis,

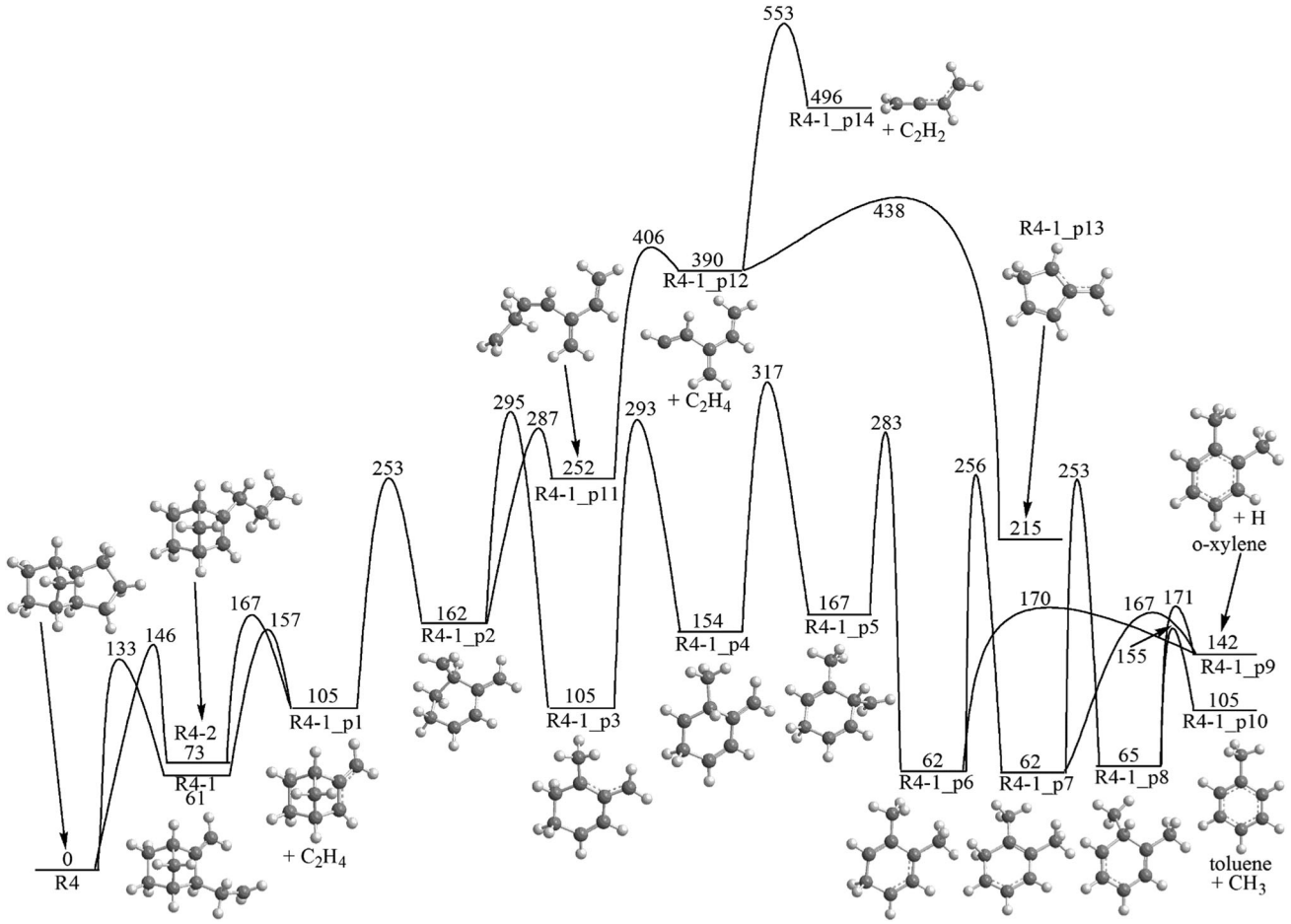

Fig. 19 Potential energy diagram for decomposition of R4-1 and R4-2. All relative energies are computed at the G3 level and are given in kJ mol^{-1}.

at least in the ALS experiments with shorter residence times in the reactor. For instance, the ethyl radical (C_2H_5), which is predominant at 1200 K, is a primary product of R4-3. At higher temperatures, this radical partially decomposes to ethylene plus atomic hydrogen. Alternatively, ethylene is produced in multiple primary and secondary fragmentation channels of R1, R4, and R6. The vinyl radical (C_2H_3) is a primary and secondary dissociation product of R1-1 and a secondary product of R1-2 and R6, but can also be formed by dehydrogenation of ethylene. Acetylene is produced in the secondary decomposition of R1-1, R1-3, R4-1, R4-2, and R5-1, and can also stem from the dehydrogenation of vinyl. Another major radical observed, allyl (C_3H_5), ubiquitously forms in multiple primary and secondary fragmentation channels of R4-5, R5-1, R6, and R1-3. The allyl radical is well known to eventually decompose to allene (C_3H_4), methylacetylene (C_3H_4), and the propargyl radical (C_3H_3),[83–85] and can also recombine with H atoms to form propene (C_3H_6), which is a minor product compared to allyl. The methyl radical is expected to form in conjunction with dihydroindane from R1-3 and R4-4 in primary channels and together with toluene in the secondary decomposition of the R4-1/R4-2 products.

The main C4 product, 1,3-butadiene (C_4H_6) can originate from R1-1, R1-3, and some other less favorable channels not discussed here (R5-3); in fact, whenever the $C_{10}H_{15}$ structure opens to a chain isomer prior its fragmentation, 1,3-butadiene tends to be the preferred product of β-scission. Its counterpart, C_6H_9, either ring closes to cyclohexenyl or eliminates ethylene producing the C_4H_5 radical, which then can form vinylacetylene (C_4H_4) or 1,2,3-butatriene (C_4H_4) by emitting a hydrogen atom (R1-1_p9 in Fig. 16 and R4-1_p14 in Fig. 19). Further dehydrogenation of both C_4H_4 isomers may be responsible for the observation of the trace diacetylene product at the highest temperature in the ALS experiment. Also, the C_4H_8 products can be formed by hydrogenation of 1,3-butadiene. Alternatively, the butadienyl radical C_4H_7 can be produced by β-scission-type acetylene loss from R5-1_p4 and this radical can then add a hydrogen atom forming 1-butene or undergo a hydrogen shift followed by hydrogen atom addition producing 2-butene. For the acyclic C5 molecules observed, ethynylallene (C_5H_4) can be obtained by dehydrogenation of 1,4-pentadien-5-yl (R1-3_p5, Fig. 18) or 1,4-pentadiene (R4-5_p2, Fig. 20, and R5-1_p2, Fig. 21), whereas 1,3-pentadiene (C_5H_8) can stem from atomic hydrogen addition to 1,4-pentadien-5-yl or isomerization of 1,4-pentadiene.

The major pyrolysis products containing five-membered rings, cyclopentene (C_5H_8) and cyclopentyl radical (C_5H_7), can be produced through favorable primary decomposition channels

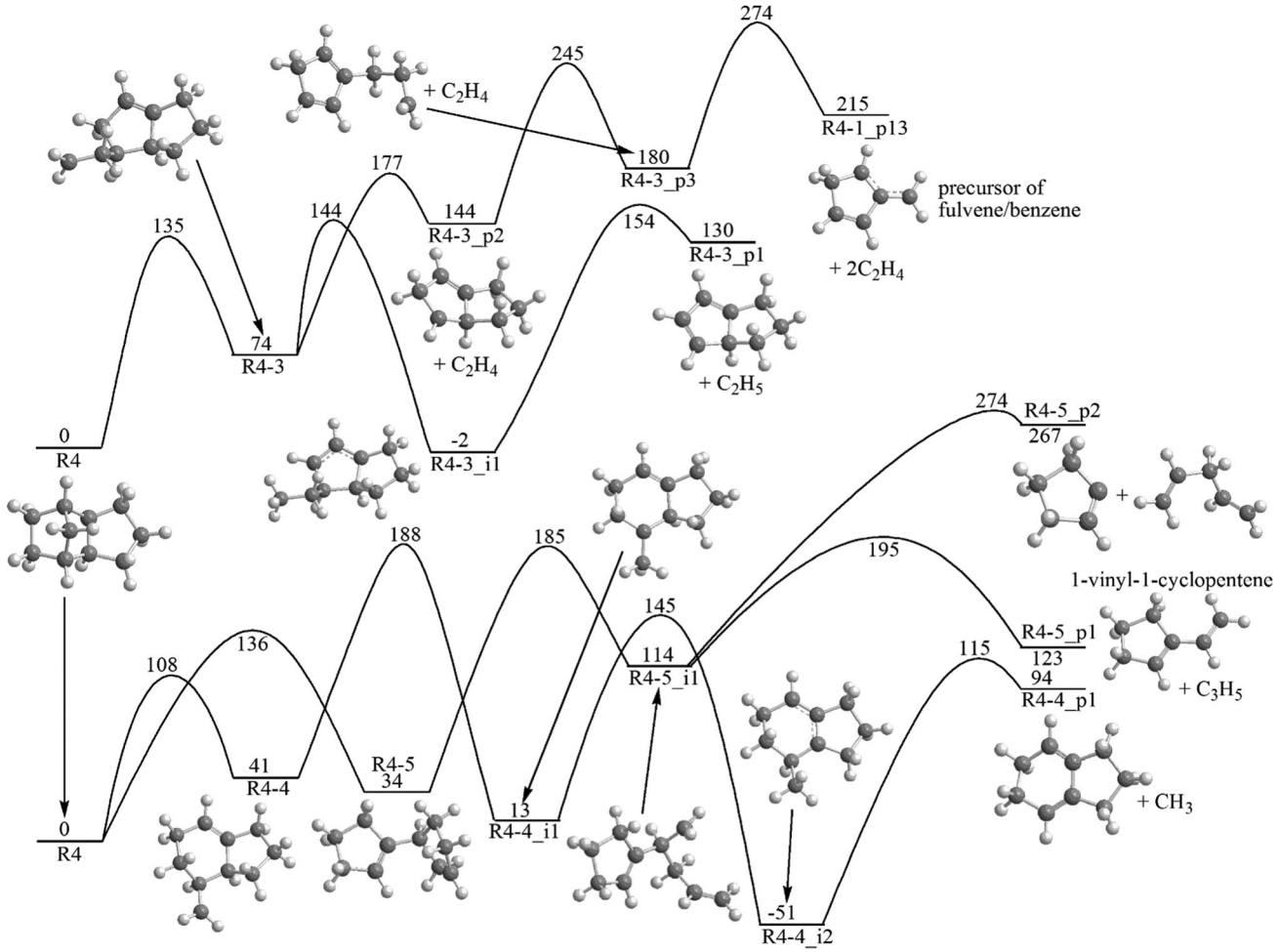

Fig. 20 Potential energy diagram for decomposition of R4-3 (top) and R4-4 and R4-5 (bottom). All relative energies are computed at the G3 level and are given in kJ mol^{-1}.

involving R1-2 and R5-1. Apparently, the cyclopentyl radical is unstable under the experimental conditions and dissociates further to cyclopentadiene (C_5H_6), which in turn can undergo one more hydrogen atom loss to the cyclopentadienyl radical (C_5H_5). Vinyl-substituted cyclopentenes R4-5_p1 and R5-1_p1 are formed as primary decomposition products of R4-5 and R5-1 and an out-of-ring C–C bond cleavage in these products will also produce a cyclopentyl radical and further cyclopentadiene. In less favorable channels, cyclopentene can be produced directly from R1-3 and cyclopentadiene can be formed as a secondary product of dissociation of R6-1_p4, which corresponds to R6-1_p1 activated by hydrogen abstraction or a C–H bond cleavage, and of R1-3_p3. Vinyl-substituted cyclopentenes can serve as precursors of such trace products as fulvenallene C_7H_6 and fulvenallenyl C_7H_5.

The most preferable pathways to the fulvene/benzene precursor R4-1_p13 is the secondary decomposition of R4-3_p2, one of the most likely decomposition products of R4-3. The R4-3_p1 product may also dissociate to a fulvene/benzene precursor but it requires initial activation by H loss/abstraction or addition. An alternative higher-barrier pathway to the fulvene/benzene precursor involves secondary dissociation of R4-1_p11. Among the other cyclic C6 species, cyclohexene and 1,3-cyclohexadiene can respectively be formed by hydrogen addition or hydrogen loss/abstraction from the cyclohexenyl radical, secondary decomposition products of R1-1 (*via* R1-1_p1) and R1-3 (*via* R-1_p2). So far, we could not locate a one-step pathway to cyclohexene. Alternatively, 1,4-cyclohexadiene is produced by elimination of the vinyl group from R1-1_p6, which in turn is formed by the ring closure in the primary decomposition products of R1-1 and R1-3. Hydrogen atom elimination in R1-1_p6 produces dihydrostyrene, which serves as a precursor of the minor styrene product. Moreover, further dehydrogenation of styrene (C_8H_8) can form the trace C_8H_6 products phenylacetylene and benzocyclobutadiene (after a four-member ring closure). 5-Methylene-1,3-cyclohexadiene stems from the decomposition of the C_9H_9 radical R6-1_p4, which is obtained by hydrogen loss/abstraction from the most favorable fragmentation product of R6, C_9H_{10} (R6-1_p1). Toluene and *o*-xylene originate from R4-1_p1, the most favorable decomposition product of R4-1 and R4-2. Removal of two hydrogen atoms from *o*-xylene can lead to the production of another C_8H_8 isomer observed, *o*-xylylene. Among larger

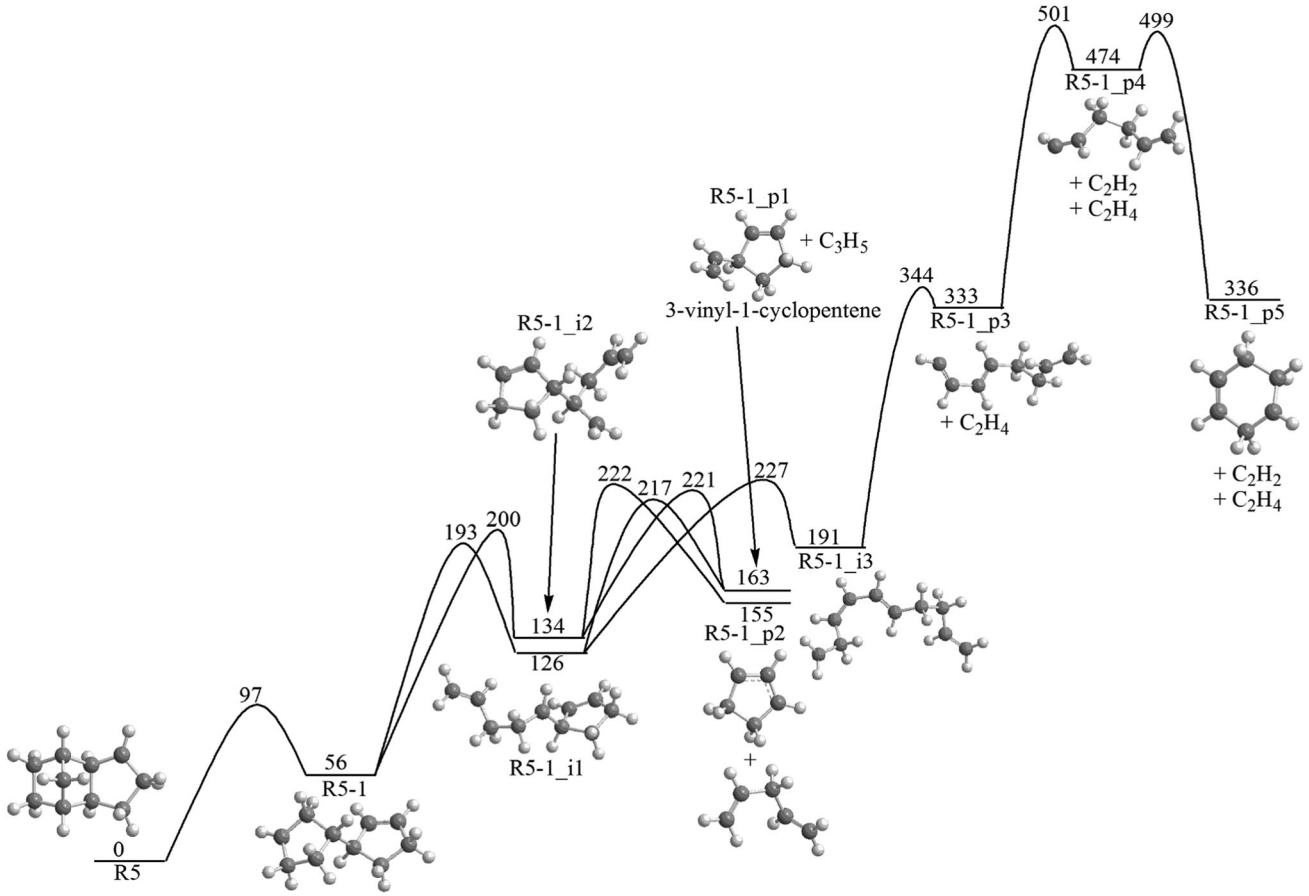

Fig. 21 Potential energy diagram for decomposition of R5-1. All relative energies are computed at the G3 level and are given in kJ mol^{-1}.

ring species, 1,3,5-cyclooctatriene is likely to originate from cyclooctadiene formed in the primary decomposition of R1-1 but may also be produced by dehydrogenation of a cyclooctadienyl radical formed through a relatively minor channel involving R5-2. Finally, indane and indene stem from dehydrogenation of dihydroindanes, the primary fragmentation products of R1-3 and R4-4. The additional PAH-type products seen in the NRLS experiment, naphthalene, acenaphthylene, and biphenyl, are likely to be due to molecular growth reactions.

A comparison of the experimental and theoretical results on the fragmentation mechanisms allowed us to identify the most favorable reaction pathways to the most important fragmentation products. In order to develop more reliable kinetic models for JP-10 pyrolysis, one needs to evaluate rate constants and relative product yields for these critical pathways and their dependence on temperature and pressure. Also, theory shows several closed-shell molecules, which are likely to be primary decomposition products, such as vinyl-cyclopentenes C_7H_{10} and their bicyclic isomer R6-1_p1, C_8H_8 (C_5H_4═$CHCHCH_2$, R1-2_p4), bicyclic C_8H_{10} (R4-3_p1), and dihydroindenes C_9H_{12}, which were not identified or even not detected experimentally. Therefore, the next step in the kinetic analysis should be the consideration of the mechanism and products of their decomposition.

In conclusion, experiments in the two pyrolytic reactors with different residence times of a few 10 μs and of 100 ms allowed us to determine the major, minor, and trace decomposition products of JP-10 and their relative yields and how they depend on the residence time with radicals less favorable to survive with increasing residence times in the reactor. At longer residence times, the predominant fragments are molecular hydrogen (H_2), ethylene (C_2H_4), propene (C_3H_6), cyclopentadiene (C_5H_6), cyclopentene (C_5H_8), fulvene (C_6H_6), and benzene (C_6H_6), but at the relatively early stages, a large fraction of radicals, such as ethyl (C_2H_5), allyl (C_3H_5), and methyl (CH_3), are produced at the expense of ethylene and propene. Eventually, the radicals react to increase the yield of the closed-shell molecules. This indicates that the oxidation mechanism will significantly depend on the time when oxygen becomes available. Further, extended residence times promote higher order reactions as evident from the naphthalene, acenaphthylene, and biphenyl products formed in the NSRL studies, which can be formed *via* phenyl – vinylacetylene,[86] naphthyl – acetylene,[87] and phenyl – benzene[88] reactions as verified in prior studies. Therefore, future studies on JP-10 decomposition should explore not only the effects of the temperature, but also systematically how the products and their branching ratios depend on the pressure and residence times in the reactor. Finally, subsequent studies should also

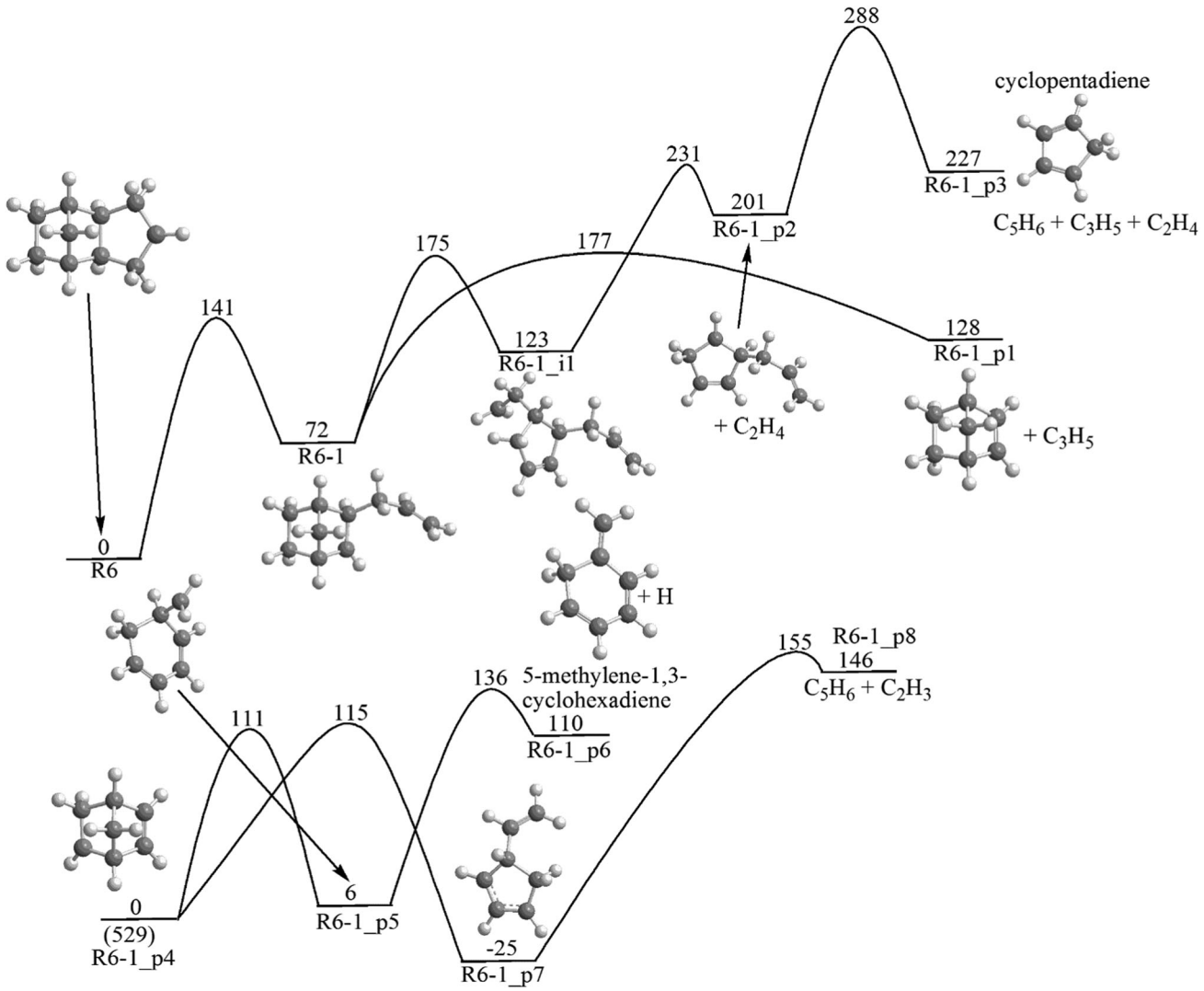

Fig. 22 Potential energy diagram for decomposition of R6 (top) and its C_7H_{10} product (R6-1_p1) activated by H loss/abstraction (bottom). All relative energies are computed at the G3 level and are given in kJ mol^{-1}.

probe the oxidation mechanisms of JP-10. Considering the complexity of the JP-10 decomposition alone, simply seeding JP-10 (at distinct seeding fractions) in molecular oxygen might provide the overall product yields of oxygen-bearing products; however, these studies will never derive the underlying reaction pathways involved in the oxidation. This requires a sophisticated investigation of the individual hydrocarbon radicals formed in the JP-10 decomposition process– as probed here – reacting with molecular oxygen in the pyrolytic reactor to ultimately decipher the reaction products of individual C1 to C6 radicals with molecular oxygen in the combustion of JP-10.

Authors contributions

R. I. Kaiser and M. Ahmed designed experiments, L. Zhao, T. Yang, T. P. Troy, and B. Xu performed experiments at the ALS, Y. Zhang, C. Cao, and J. Zou performed experiments at the NRLS, J. Alarcon, D. Belisario-Lara, and A. M. Mebel carried out theoretical calculations; L. Zhao, R. I. Kaiser, M. Ahmed, and A. M. Mebel wrote the manuscript, which was read, revised, and approved by all co-authors.

Acknowledgements

This project is supported by the Air Force Office of Scientific Research (AFOSR) under Grant Number FA9550-15-1-0011 (LZ, TY, AMM, RIK). The work of M. A., B. X., and T. P. at the Advanced Light Source was supported by the Director, Office of Science, Office of Basic Energy Sciences, of the U.S. Department of Energy under Contract No. DE-AC02-05CH11231, through the Chemical Sciences Division.

References

1 A. Osmont, I. Gokalp and L. Catoire, *Propellants, Explos., Pyrotech.*, 2006, **31**, 343–354.

2 H. Chung, C. Chen, R. Kremer, J. Boulton and G. Burdette, *Energy Fuels*, 1999, **13**, 641–649.
3 L. Q. Maurice, H. Lander, T. Edwards and W. Harrison, *Fuel*, 2001, **80**, 747–756.
4 B. Van Devener and S. L. Anderson, *Energy Fuels*, 2006, **20**, 1886–1894.
5 C. W. Gao, A. G. Vandeputte, N. W. Yee, W. H. Green, R. E. Bonomi, G. R. Magoon, H.-W. Wong, O. O. Oluwole, D. K. Lewis and N. M. Vandewiele, *Combust. Flame*, 2015, **162**, 3115–3129.
6 S. Nakra, R. J. Green and S. L. Anderson, *Combust. Flame*, 2006, **144**, 662–674.
7 N. M. Vandewiele, G. R. Magoon, K. M. Van Geem, M.-F. Reyniers, W. H. Green and G. B. Marin, *Energy Fuels*, 2014, **28**, 4976–4985.
8 O. Herbinet, B. Sirjean, R. Bounaceur, R. Fournet, F. Battin-Leclerc, G. Scacchi and P.-M. Marquaire, *J. Phys. Chem. A*, 2006, **110**, 11298–11314.
9 P. N. Rao and D. Kunzru, *J. Anal. Appl. Pyrolysis*, 2006, **76**, 154–160.
10 R. Striebich and J. Lawrence, *J. Anal. Appl. Pyrolysis*, 2003, **70**, 339–352.
11 K. Wohlwend, L. Maurice, T. Edwards, R. Striebich, M. Vangsness and A. Hill, *J. Propul. Power*, 2001, **17**, 1258–1262.
12 Y. Xing, W. Fang, W. Xie, Y. Guo and R. Lin, *Ind. Eng. Chem. Res.*, 2008, **47**, 10034–10040.
13 G. Li, C. Zhang, H. Wei, H. Xie, Y. Guo and W. Fang, *Fuel*, 2016, **163**, 148–156.
14 T. J. Bruno, M. L. Huber, A. Laesecke, E. W. Lemmon and R. A. Perkins, *Tech. Rep. NISTIR*, 2006, **6640**, 325.
15 S. H. Park, C. H. Kwon, J. Kim, B. H. Chun, J. W. Kang, J. S. Han, B. H. Jeong and S. H. Kim, *Ind. Eng. Chem. Res.*, 2010, **49**, 8319–8324.
16 H. Li, G. Liu, R. Jiang, L. Wang and X. Zhang, *Combust. Flame*, 2015, **162**, 2177–2190.
17 N. M. Vandewiele, G. R. Magoon, K. M. Van Geem, M.-F. Reyniers, W. H. Green and G. B. Marin, *Energy Fuels*, 2014, **29**, 413–427.
18 L. Yue, H.-J. Xie, X.-M. Qin, X.-X. Lu and W.-J. Fang, *J. Mol. Model.*, 2013, **19**, 5355–5365.
19 K. Chenoweth, A. C. T. van Duin, S. Dasgupta and W. A. Goddard Iii, *J. Phys. Chem. A*, 2009, **113**, 1740–1746.
20 G. R. Magoon, J. Aguilera-Iparraguirre, W. H. Green, J. J. Lutz, P. Piecuch, H. W. Wong and O. O. Oluwole, *Int. J. Chem. Kinet.*, 2012, **44**, 179–193.
21 J. M. Hudzik, R. Asatryan and J. W. Bozzelli, *J. Phys. Chem. A*, 2010, **114**, 9545–9553.
22 J. M. Hudzik, A. Castillo and J. W. Bozzelli, *J. Phys. Chem. A*, 2015, **119**, 9857–9878.
23 M. J. Zehe and R. L. Jaffe, *J. Org. Chem.*, 2010, **75**, 4387–4391.
24 S. S. Cheng, K. F. Liou and Y. T. Lin, *J. Chin. Chem. Soc.*, 1986, **33**, 335–340.
25 O. Prakash, R. K. Tiwari, S. L. Kalra and P. S. Venkataramani, *Indian J. Chem. Technol.*, 1995, **2**, 295–297.
26 D. F. Davidson, D. C. Horning, J. T. Herbon and R. K. Hanson, *Proc. Combust. Inst.*, 2000, **28**, 1687–1692.
27 S. C. Li, B. Varatharajan and F. A. Williams, *AIAA J.*, 2001, **39**, 2351–2356.
28 D. W. Mikolaitis, C. Segal and A. Chandy, *J. Propul. Power*, 2003, **19**, 601–606.
29 F. Parsinejad, C. Arcari and H. Metghalchi, *Combust. Sci. Technol.*, 2006, **178**, 975–1000.
30 C. Q. Jiao, C. A. DeJoseph and A. Garscadden, *Int. J. Mass Spectrom.*, 2007, **266**, 92–96.
31 S. Wang, H.-J. Gou, B.-C. Fan, Y.-Z. He, S.-T. Zhang and J.-P. Cui, *Chin. J. Chem. Phys.*, 2007, **20**, 48–52.
32 Y. Xing, Y. S. Guo, D. Li, W. J. Fang and R. S. Lin, *Energy Fuels*, 2007, **21**, 1048–1051.
33 F. J. Yang, Y. S. Guo, Y. Xing, D. Li, W. J. Fang and R. S. Lin, *J. Chem. Eng. Data*, 2008, **53**, 2237–2240.
34 X. H. Su, H. M. Hou, G. Li, R. S. Lin and S. L. Cai, *Acta Chim. Sin.*, 2009, **67**, 587–592.
35 R. Seiser, U. Niemann and K. Seshadri, *Proc. Combust. Inst.*, 2011, **33**, 1045–1052.
36 F. Guo, X. L. Cheng and H. Zhang, *Combust. Sci. Technol.*, 2012, **184**, 1233–1243.
37 K. H. H. Goh, P. Geipel, F. Hampp and R. P. Lindstedt, *Proc. Combust. Inst.*, 2013, **34**, 3311–3318.
38 L. Türker, S. Variş and Ç. Çelik Bayar, *Fuel*, 2013, **104**, 128–132.
39 X. M. Qin, H. J. Xie, L. Yue, X. X. Lu and W. J. Fang, *J. Mol. Model.*, 2014, **20**, 8.
40 F. T. Zhang, R. I. Kaiser, V. V. Kislov, A. M. Mebel, A. Golan and M. Ahmed, *J. Phys. Chem. Lett.*, 2011, **2**, 1731–1735.
41 F. T. Zhang, R. I. Kaiser, A. Golan, M. Ahmed and N. Hansen, *J. Phys. Chem. A*, 2012, **116**, 3541–3546.
42 R. I. Kaiser, L. Belau, S. R. Leone, M. Ahmed, Y. M. Wang, B. J. Braams and J. M. Bowman, *ChemPhysChem*, 2007, **8**, 1236–1239.
43 R. I. Kaiser, A. Mebel, O. Kostko and M. Ahmed, *Chem. Phys. Lett.*, 2010, **485**, 281–285.
44 R. I. Kaiser, P. Maksyutenko, C. Ennis, F. T. Zhang, X. B. Gu, S. P. Krishtal, A. M. Mebel, O. Kostko and M. Ahmed, *Faraday Discuss.*, 2010, **147**, 429–478.
45 R. I. Kaiser, B. J. Sun, H. M. Lin, A. H. H. Chang, A. M. Mebel, O. Kostko and M. Ahmed, *Astrophys. J.*, 2010, **719**, 1884–1889.
46 O. Kostko, J. Zhou, B. J. Sun, J. S. Lie, A. H. H. Chang, R. I. Kaiser and M. Ahmed, *Astrophys. J.*, 2010, **717**, 674–682.
47 R. I. Kaiser, S. P. Krishtal, A. M. Mebel, O. Kostko and M. Ahmed, *Astrophys. J.*, 2012, **761**, 178–184.
48 A. Golan, M. Ahmed, A. M. Mebel and R. I. Kaiser, *Phys. Chem. Chem. Phys.*, 2013, **15**, 341–347.
49 D. S. Parker, R. I. Kaiser, T. P. Troy and M. Ahmed, *Angew. Chem., Int. Ed.*, 2014, **53**, 7740–7744.
50 F. Qi, R. Yang, B. Yang, C. Q. Huang, L. X. Wei, J. Wang, L. S. Sheng and Y. W. Zhang, *Rev. Sci. Instrum.*, 2006, **77**, 084101.
51 B. Yang, Y. Y. Li, L. X. Wei, C. Q. Huang, J. Wang, Z. Y. Tian, R. Yang, L. S. Sheng, Y. W. Zhang and F. Qi, *Proc. Combust. Inst.*, 2007, **31**, 555–563.

52 B. Yang, P. Oßwald, Y. Li, J. Wang, L. Wei, Z. Tian, F. Qi and K. Kohse-Höinghaus, *Combust. Flame*, 2007, **148**, 198–209.

53 Y. Y. Li, L. D. Zhang, Z. Y. Tian, T. Yuan, J. Wang, B. Yang and F. Qi, *Energy Fuels*, 2009, **23**, 1473–1485.

54 Y. Y. Li, L. D. Zhang, Z. Y. Tian, T. Yuan, K. W. Zhang, B. Yang and F. Qi, *Proc. Combust. Inst.*, 2009, **32**, 1293–1300.

55 L. D. Zhang, J. H. Cai, T. C. Zhang and F. Qi, *Combust. Flame*, 2010, **157**, 1686–1697.

56 P. Oßwald, H. Güldenberg, K. Kohse-Höinghaus, B. Yang, T. Yuan and F. Qi, *Combust. Flame*, 2011, **158**, 2–15.

57 F. Qi, *Proc. Combust. Inst.*, 2013, **34**, 33–63.

58 O. Kostko, B. Bandyopadhyay and M. Ahmed, *Annu. Rev. Phys. Chem.*, 2016, **67**, 19–40.

59 Q. Guan, K. N. Urness, T. K. Ormond, D. E. David, G. B. Ellison and J. W. Daily, *Int. Rev. Phys. Chem.*, 2014, **33**, 447–487.

60 T. C. Zhang, J. Wang, T. Yuan, X. Hong, L. D. Zhang and F. Qi, *J. Phys. Chem. A*, 2008, **112**, 10487–10494.

61 T. C. Zhang, L. D. Zhang, X. Hong, K. W. Zhang, F. Qi, C. K. Law, T. H. Ye, P. H. Zhao and Y. L. Chen, *Combust. Flame*, 2009, **156**, 2071–2083.

62 J. H. Cai, L. D. Zhang, F. Zhang, Z. D. Wang, Z. J. Cheng, W. H. Yuan and F. Qi, *Energy Fuels*, 2012, **26**, 5550–5568.

63 Z. Wang, Z. Cheng, W. Yuan, J. Cai, L. Zhang, F. Zhang, F. Qi and J. Wang, *Combust. Flame*, 2012, **159**, 2243–2253.

64 Y. J. Zhang, J. H. Cai, L. Zhao, J. Z. Yang, H. F. Jin, Z. J. Cheng, Y. Y. Li, L. D. Zhang and F. Qi, *Combust. Flame*, 2012, **159**, 905–917.

65 Y. Y. Li, L. D. Zhang, Z. D. Wang, L. L. Ye, J. H. Cai, Z. J. Cheng and F. Qi, *Proc. Combust. Inst.*, 2013, **34**, 1739–1748.

66 Z. Y. Zhou, X. W. Du, J. Z. Yang, Y. Z. Wang, C. Y. Li, S. Wei, L. L. Du, Y. Y. Li, F. Qi and Q. P. Wang, *J. Synchrotron Radiat.*, 2016, **23**, 1035–1045.

67 CHEMKIN-PRO 15092, Reaction Design, San Diego, 2009.

68 T. A. Cool, A. McIlroy, F. Qi, P. R. Westmoreland, L. Poisson, D. S. Peterka and M. Ahmed, *Rev. Sci. Instrum.*, 2005, **76**, 094102.

69 T. A. Cool, J. Wang, K. Nakajima, C. A. Taatjes and A. McIlroy, *Int. J. Mass Spectrom.*, 2005, **247**, 18–27.

70 L. Zhao, T. Yang, R. I. Kaiser, T. P. Troy, M. Ahmed, D. Belisario-Lara, J. M. Ribeiro and A. M. Mebel, *J. Phys. Chem. A*, 2017, **121**, 1261–1280.

71 L. Zhao, T. Yang, R. I. Kaiser, T. P. Troy, M. Ahmed, J. M. Ribeiro, D. Belisario-Lara and A. M. Mebel, *J. Phys. Chem. A*, 2017, **121**, 1281–1297.

72 *Photonionization Cross Section Database (Version 2.0)*, National Synchrotron Radiation Laboratory, Hefei, China, 2017, http://flame.nsrl.ustc.edu.cn/database/.

73 K. N. Urness, Q. Guan, A. Golan, J. W. Daily, M. R. Nimlos, J. F. Stanton, M. Ahmed and G. B. Ellison, *J. Chem. Phys.*, 2013, **139**, 124305.

74 T. A. Cool, K. Nakajima, C. A. Taatjes, A. McIlroy, P. R. Westmoreland, M. E. Law and A. Morel, *Proc. Combust. Inst.*, 2005, **30**, 1681–1688.

75 A. D. Becke, *J. Chem. Phys.*, 1993, **98**, 5648–5652.

76 C. Lee, W. Yang and R. G. Parr, *Phys. Rev. B: Condens. Matter Mater. Phys.*, 1988, **37**, 785.

77 A. G. Baboul, L. A. Curtiss, P. C. Redfern and K. Raghavachari, *J. Chem. Phys.*, 1999, **110**, 7650–7657.

78 L. A. Curtiss, K. Raghavachari, P. C. Redfern, A. G. Baboul and J. A. Pople, *Chem. Phys. Lett.*, 1999, **314**, 101–107.

79 L. A. Curtiss, K. Raghavachari, P. C. Redfern, V. Rassolov and J. A. Pople, *J. Chem. Phys.*, 1998, **109**, 7764–7776.

80 M. J. Frisch, G. W. Trucks, H. B. Schlegel, G. E. Scuseria, M. A. Robb, J. R. Cheeseman, G. Scalmani, V. Barone, B. Mennucci, G. A. Petersson, H. Nakatsuji, M. Caricato, X. Li, H. P. Hratchian, A. F. Izmaylov, J. Bloino, G. Zheng, J. L. Sonnenberg, M. Hada, M. Ehara, K. Toyota, R. Fukuda, J. Hasegawa, M. Ishida, T. Nakajima, Y. Honda, O. Kitao, H. Nakai, T. Vreven, J. A. Montgomery Jr, J. E. Peralta, F. Ogliaro, M. Bearpark, J. J. Heyd, E. Brothers, K. N. Kudin, V. N. Staroverov, T. Keith, R. Kobayashi, J. Normand, K. Raghavachari, A. Rendell, J. C. Burant, S. S. Iyengar, J. Tomasi, M. Cossi, N. Rega, J. M. Millam, M. Klene, J. E. Knox, J. B. Cross, V. Bakken, C. Adamo, J. Jaramillo, R. Gomperts, R. E. Stratmann, O. Yazyev, A. J. Austin, R. Cammi, C. Pomelli, J. W. Ochterski, R. L. Martin, K. Morokuma, V. G. Zakrzewski, G. A. Voth, P. Salvador, J. J. Dannenberg, S. Dapprich, A. D. Daniels, O. Farkas, J. B. Foresman, J. V. Ortiz, J. Cioslowski and D. J. Fox, *Gaussian, 09, Revision. 1*, Gaussian Inc., Wallingford CT, 2009.

81 H. J. Werner, P. J. Knowles, G. Knizia, F. R. Manby, M. Schütz, P. Celani, W. Györffy, D. Kats, T. Korona, R. Lindh, A. Mitrushenkov, G. Rauhut, K. R. Shamasundar, T. B. Adler, R. D. Amos, A. Bernhardsson, A. Berning, D. L. Cooper, M. J. O. Deegan, A. J. Dobbyn, F. Eckert, E. Goll, C. Hampel, A. Hesselmann, G. Hetzer, T. Hrenar, G. Jansen, C. Köppl, Y. Liu, A. W. Lloyd, R. A. Mata, A. J. May, S. J. McNicholas, W. Meyer, M. E. Mura, A. Nicklaß, D. P. O'Neill, P. Palmieri, D. Peng, K. Pflüger, R. Pitzer, M. Reiher, T. Shiozaki, H. Stoll, A. J. Stone, R. Tarroni, T. Thorsteinsson and M. Wang, *MOLPRO, version 2010.1*, a package of ab initio programs, http://www.molpro.net.

82 J. M. Bowman and B. C. Shepler, *Annu. Rev. Phys. Chem.*, 2011, **62**, 531–553.

83 J. A. Miller, J. P. Senosiain, S. J. Klippenstein and Y. Georgievskii, *J. Phys. Chem. A*, 2008, **112**, 9429–9438.

84 B. S. Narendrapurapu, A. C. Simmonett, H. F. Schaefer III, J. A. Miller and S. J. Klippenstein, *J. Phys. Chem. A*, 2011, **115**, 14209–14214.

85 N. Hansen, J. A. Miller, P. R. Westmoreland, T. Kasper, K. Kohse-Höinghaus, J. Wang and T. A. Cool, *Combust. Flame*, 2009, **156**, 2153–2164.

86 X. Gu, F. Zhang, Y. Guo and R. I. Kaiser, *Angew. Chem., Int. Ed.*, 2007, **46**, 6866–6869.

87 D. S. Parker, R. Kaiser, B. Bandyopadhyay, O. Kostko, T. P. Troy and M. Ahmed, *Angew. Chem.*, 2015, **127**, 5511–5514.

88 F. Zhang, X. Gu and R. I. Kaiser, *J. Chem. Phys.*, 2008, **128**, 084315.